NASA/TM–20250002895

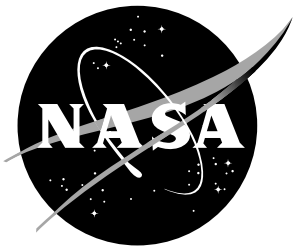

Surface Roughness Measurements on the NASA Juncture Flow Model: 2022 Test Entry

Andrew N. Leidy
Langley Research Center, Hampton, Virginia

March 2025

NASA STI Program. . . in Profile

Since its founding, NASA has been dedicated to the advancement of aeronautics and space science. The NASA scientific and technical information (STI) program plays a key part in helping NASA maintain this important role.

The NASA STI Program operates under the auspices of the Agency Chief Information Officer. It collects, organizes, provides for archiving, and disseminates NASA's STI. The NASA STI Program provides access to the NASA Aeronautics and Space Database and its public interface, the NASA Technical Report Server, thus providing one of the largest collection of aeronautical and space science STI in the world. Results are published in both non-NASA channels and by NASA in the NASA STI Report Series, which includes the following report types:

- TECHNICAL PUBLICATION. Reports of completed research or a major significant phase of research that present the results of NASA programs and include extensive data or theoretical analysis. Includes compilations of significant scientific and technical data and information deemed to be of continuing reference value. NASA counterpart of peer-reviewed formal professional papers, but having less stringent limitations on manuscript length and extent of graphic presentations.
- TECHNICAL MEMORANDUM. Scientific and technical findings that are preliminary or of specialized interest, e.g., quick release reports, working papers, and bibliographies that contain minimal annotation. Does not contain extensive analysis.
- CONTRACTOR REPORT. Scientific and technical findings by NASA-sponsored contractors and grantees.
- CONFERENCE PUBLICATION. Collected papers from scientific and technical conferences, symposia, seminars, or other meetings sponsored or co-sponsored by NASA.
- SPECIAL PUBLICATION. Scientific, technical, or historical information from NASA programs, projects, and missions, often concerned with subjects having substantial public interest.
- TECHNICAL TRANSLATION. English-language translations of foreign scientific and technical material pertinent to NASA's mission.

Specialized services also include organizing and publishing research results, distributing specialized research announcements and feeds, providing information desk and personal search support, and enabling data exchange services.

For more information about the NASA STI Program, see the following:

- Access the NASA STI program home page at `http://www.sti.nasa.gov`
- E-mail your question to `help@sti.nasa.gov`
- Phone the NASA STI Information Desk at 757-864-9658
- Write to:
  NASA STI Information Desk
  Mail Stop 148
  NASA Langley Research Center
  Hampton, VA 23681-2199

NASA/TM–20250002895

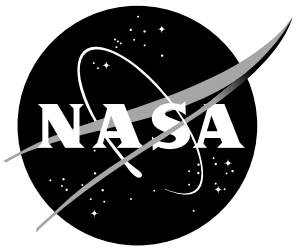

Surface Roughness Measurements on the NASA Juncture Flow Model: 2022 Test Entry

Andrew N. Leidy
Langley Research Center, Hampton, Virginia

National Aeronautics and
Space Administration

Langley Research Center
Hampton, Virginia 23681-2199

March 2025

The use of trademarks or names of manufacturers in this report is for accurate reporting and does not constitute an official endorsement, either expressed or implied, of such products or manufacturers by the National Aeronautics and Space Administration.

Available from:

NASA STI Program / Mail Stop 148
NASA Langley Research Center
Hampton, VA 23681-2199
Fax: 757-864-6500

Abstract

Surface roughness measurements were made on the upper surface of both wings of the NASA Juncture Flow model prior to its entry into the NASA Langley 14- by 22-Foot Subsonic Tunnel in January 2022. Measurements were acquired using a stylus profilometer with a 2-µm radius tip. Roughness parameters were evaluated in accordance with the ASME B46.1-2002 standards. The root-mean-square roughness levels, considering all measured regions, were 3.104 ± 0.016 µm and 3.532 ± 0.015 µm on the port and starboard wings, respectively. Roughness spectra were also provided since wavelengths between 3–5 mm were computationally shown to amplify the crossflow instability. More prominent spectral peaks were observed on the leading edge of the port wing compared to the starboard wing. Additional profiles were taken with the model installed in the tunnel following the boundary-layer transition measurements. The measurements within the tunnel focused on evaluating the step height and gap width at the interface between the wing and fairing.

Contents

1 Introduction **7**

2 Measurement Procedure **7**
2.1 Stylus Profilometry 8
2.2 Optical Microscope Consideration 8

3 Methods of Analysis **9**
3.1 Roughness Parameters 10
3.2 Step Height 11

4 Results **12**
4.1 Roughness Parameters 12
4.2 Roughness Spectra 13
4.3 Wing/Fairing Interface Characterization 14

5 Summary **15**

List of Tables

1 Scan regions on port wing. 17
2 Scan regions on starboard wing. 17
3 Wing/fairing interface scan locations. 18
4 Measured R_a on the port wing. Scans were processed using a quadratic-fit subtraction. 18
5 Measured R_a on the port wing. Scans were processed using a linear-fit subtraction. 19
6 Measured R_a on the starboard wing. Scans were processed using a quadratic-fit subtraction. 19
7 Measured R_a on the starboard wing. Scans were processed using a linear-fit subtraction. 20
8 Measured R_q on the port wing. Scans were processed using a quadratic-fit subtraction. 20
9 Measured R_q on the port wing. Scans were processed using a linear-fit subtraction. 21
10 Measured R_q on the starboard wing. Scans were processed using a quadratic-fit subtraction. 21
11 Measured R_q on the starboard wing. Scans were processed using a linear-fit subtraction. 22
12 Measured R_{sk} and R_{ku} on the port wing. 22
13 Measured R_{sk} and R_{ku} on the starboard wing. 23
14 Measured parameters at the wing/fairing interface. 23

List of Figures

1 Top view of model wing geometry with regions of surface roughness measurements on the port and starboard sides 24
2 Top view of the wing on the port side of the model 25
3 Comparison scans on hatch 26
4 Steps for processing roughness from a sample spanwise scan in the p1LE region 27
5 Steps for processing roughness from a sample chordwise scan in the p1LE region 28
6 Power spectral density plots featuring different polynomial form subtractions 29
7 Comparison between the mean sampling length and mean full PSD plots from scans in the p1LE region 29
8 Sample scan of the wing/fairing interface and elements for determining the gap features 30
9 Histograms of R_a values on the port wing in regions near the leading edge 30
10 Histograms of R_a values on the port wing in regions near the middle of the chord 31
11 Histograms of R_a values on the starboard wing in regions near the leading edge 31
12 Histograms of R_a values on the starboard wing in regions near the middle of the chord 32
13 Histograms of R_q values on the port wing in regions near the leading edge 32
14 Histograms of R_q values on the port wing in regions near the middle of the chord 33
15 Histograms of R_q values on the starboard wing in regions near the leading edge 33
16 Histograms of R_q values on the starboard wing in regions near the middle of the chord 34
17 PSD comparison for full scans performed in the chordwise and spanwise directions with linear and quadratic form subtractions 34
18 PSD comparison for full scans performed on the port wing near the leading edge and in the spanwise direction 35
19 PSD comparison for full scans performed on the starboard wing near the leading edge and in the spanwise direction 35
20 PSD comparison for full scans performed on the port wing near the leading edge and in the chordwise direction 36
21 PSD comparison for full scans performed on the port wing near midchord and in the spanwise direction 36
22 PSD comparison for full scans performed on the port wing near midchord and in the chordwise direction 37
23 PSD comparison for full scans performed on the starboard wing near the leading edge and in the chordwise direction 37

24 PSD comparison for full scans performed on the starboard wing near midchord and in the spanwise direction 38
25 PSD comparison for full scans performed on the starboard wing near midchord and in the chordwise direction 38
26 PSD comparison for sampling length scans performed on the port wing near the leading edge 39
27 PSD comparison for sampling length scans performed on the port wing near the midchord 39
28 PSD comparison for sampling length scans performed on the starboard wing near the leading edge 40
29 PSD comparison for sampling length scans performed on the starboard wing near the midchord 40

Nomenclature

b	model half span, 1663.5 mm
c	local chord length
L_r	roughness sampling length, 2.5 mm
n	number of points in a sample
R_a	arithmetic-mean roughness height
R_{ku}	kurtosis of the roughness profile
R_q	root-mean-square roughness height
R_{sk}	skewness of the roughness profile
s	stylus traversing coordinate
x'	local streamwise coordinate from wing leading edge
X	body-fixed streamwise coordinate, X=0 at nose
Y	body-fixed spanwise coordinate, Y=0 at plane of symmetry
$z(s)$	roughness profile height function
Δs	spacing between sample points
λ	wavelength
λ_c	cutoff wavelength

1 Introduction

The NASA Juncture Flow model has been repeatedly tested in the NASA Langley 14- by 22-Foot Subsonic Tunnel with the primary goal of producing validation data of the flow at the trailing edge of the wing-fuselage junction [1]. The first two entries, in 2017–2018 [2–4] and 2020 [5], used the DLR-F6 wings, and had a sizable region of separated flow at the junction that was probed with laser Doppler velocimetry (LDV) [2] and particle image velocimetry (PIV) [4] systems. The wings were replaced prior to the 2022 entry with those having symmetric airfoils. The airfoils reduced in thickness moving outboard, merging from a NACA 0015 at the root, to a NACA 0012 at the wing break, to a NACA 0010 near the tip. Each wing was swept 37.3 deg, and the upstream wing-fuselage junction was smoothly merged with a fairing (also called a leading-edge extension, strake, or horn). The as-designed model half span was 1663.5 mm, and the as-designed chord length at the planform break was 580.716 mm. The wings were not previously tested and were coated in flat-black, epoxy-based paint. To maximize emissivity for infrared thermography (IR) measurements, the paint was not polished.

Boundary-layer transition measurements on the untripped symmetric airfoil wings [6] were a focus of the January 2022 test entry and were made just prior to the tripped-wing off-body flow measurements at the wing-fuselage junction [7, 8]. Results obtained from the transition portion of the entry were compared with several transition models to assess their effectiveness. The transition front was measured on both wings using IR for angles of incidence ranging from -10 to 10 deg. Two different transition mechanisms expressed varying dominance depending on the angle of incidence (α) of the model. Growth of the Tollmien-Schlichting instability led to transition on the wings for positive α values. The spanwise pressure gradient from the wing sweep enabled the amplification of the crossflow instability. The effect of stationary crossflow on the transition front was observed on the inboard portion of each wing for $\alpha < -2$ deg, and stationary crossflow became the dominant transition mechanism over the full wingspan for $\alpha < -5$ deg [6]. Computations showed that stationary crossflow wavelengths between 3–5 mm were most unstable, so characterizing the surface roughness was critical due to its potential to amplify the instability.

Section 2 describes the process of making measurements using a stylus profilometer. Section 3 details the methods of analysis for computing the surface roughness values and the step height between the wing and fairing. Section 4 reports the results, and Section 5 presents a brief summary.

2 Measurement Procedure

Surface measurements were made on both wings of the Juncture Flow model using a stylus profilometer. Subsection 2.1 will detail the procedure for making measurements using the stylus. Subsection 2.2 will discuss why the stylus was used rather than an optical microscope.

2.1 Stylus Profilometry

The stylus profilometer unit was set in a fixed position on the wing for each scan, while the stylus probe traversed over the model surface to acquire the data. Each scan was 25.4 mm, which was the maximum scan length that the device could make. Effort was made to level the device and center the measurements near zero to maximize the precision of the measurements. Raw profile height measurements were output from the device; no computational filtering was done internally. The shape of the stylus tip was a 60-deg cone with a nominal 2-µm radius, and height data were sampled every $\Delta s = 1.0$ µm of stylus travel. The height values are resolved to 0.01 µm. The profilometer was calibrated prior to the measurements using a 2.970 µm arithmetic-mean-roughness (R_a) precision reference specimen from the manufacturer.

Measurements were made in six different regions on each wing. These regions are sketched in Fig. 1, and the coordinate bounds of each region on the port wing and starboard wing are listed in Table 1 and Table 2, respectively. At least 30 scans directed chordwise and 30 scans directed parallel to the leading edge were made in each region. Note that the label "spanwise" is given to the scans that were made parallel to the leading edge although only a component is truly in the spanwise direction due to the wing sweep. The measurements were independent of each other in that the device body was physically shifted after measuring each profile.

The surface roughness measurements were made prior to installation in the 14- by 22-Foot tunnel. Additional measurements were made within the tunnel following the boundary-layer transition portion of the test entry. The focus of the in-situ measurements was on the interface between the wing and fairing. The fairing (Fig. 2), blends the fuselage and wing geometries near the wing root. Room-temperature-vulcanizing (RTV) silicone was applied to the mating surfaces during assembly, and the resulting steps and gaps are quantified herein. The scans for the interface characterization were shorter in length at 15 mm, with data sampled every 0.5 µm of stylus travel. The interface scan locations are summarized in Table 3.

2.2 Optical Microscope Consideration

Initially, consideration was made for taking structured-light-based optical measurements in addition to, or instead of, the stylus profilometer measurements. The primary benefit of the optical measurements is that a 2D mapping of surface height can be obtained rather than a collection of individual linear profiles. However, the stylus measurements gained favor for several reasons. First, the stylus was better suited to make the measurements given the large scale of the model. The structured-light-based optical device required that the sample be placed on or just above a traversing stage, and the wings were too large for that positioning to be practical. Laser-based scanning measurements were made of the as-built geometry and position of the model within the test section, but those measurements were not precise enough to evaluate the surface roughness of the wings. Another means of using the structured-light-based optical device involved casting molds of the surface, which could be brought to the machine to measure a negative of the surface rough-

ness. We decided against that option since preliminary measurements on the upper hatch suggested inconsistencies based on sample directionality.

Scans were taken over the same general area of the hatch using both the stylus and the optical device. The device was set to its highest magnification (×160) to obtain scans with the greatest spatial resolution (1.85 µm/px). Note that this is larger than the 1.0 µm sample spacing of the stylus but is comparable in scale to the 2 µm radius of the stylus tip, which effectively serves as a long pass filter. Two different 688 × 688 pixel optical scans were made, with the second scan over the same area but with the sample rotated 90 deg. Each optical scan was parsed into 688 (688 × 1 pixel) arrays (columns) and also 688 (1 × 688 pixel) arrays (rows). The surface roughness spectra were computed for each 1D array and averaged over the 688 arrays. This was done for each scan orientation and parsing direction, and the averaged spectra are shown in Fig. 3. A spectrum representing 600 averages from stylus measurements is included for comparison. For reference, the processing parameters (described in Subsection 3.1) are $L_r = 1.2$ mm and $\lambda_c = 0.8$ mm. Ultimately, the averaged spectra indicate that the direction of the parsing has a larger impact on the spectra than the 90-deg rotation of the model, i.e., the sample surface roughness is approximately isotropic, but the surface height values output from the optical machine have directional dependence. The spectral shape for the data split into columns is similar to that obtained from the stylus; however, the spectra for the data split into rows appear high for very short wavelengths ($\lambda < 30$ µm) and indicate a false local maxium near $\lambda = 60$ µm. The alignment is better between the different diagnostic and processing methods for $\lambda > 100$ µm. The device limitation in measuring relatively small height value differences is likely related to the directionality in which light is projected from the measurement head. Further investigation is needed to determine optimal measurement and analysis techniques when using the device.

The limited scan length also prevented the optical device from being a viable option. Computational results suggested that the crossflow instability would be most amplified by roughness with a wavelength in the 3–5 mm range. Therefore, the scan length would need to be several times those values to have confidence in the spectral content at those long wavelengths. Additionally, a 1.2 mm scan is not long enough to perform the prescribed filtering of the ASME B46.1-2002 standard. The filtering methods are described in Subsection 3.1. The optical device is capable of 24.0 × 18.0 mm scans at 12× magnification, but the spatial resolution becomes 23.5 µm/px, which would reduce spectral content at lower wavelengths and the effective rms value. Finally, it should also be noted that the data from the optical device consistently produces higher rms roughness values than those from the stylus profilometer.

3 Methods of Analysis

This section presents the algorithms used for data analysis. Subsection 3.1 provides the steps for estimating the model surface roughness parameters. Subsection 3.2 provides the method for approximating the step height and gap width at the interface

between the wing and fairing.

3.1 Roughness Parameters

The roughness parameters for each scan were evaluated using the following steps. The effects of the processing for spanwise (p1LE) and chordwise (p1LEc) scans near the leading edge are depicted in Figs. 4 and 5, respectively.

- Break each 25.4 mm scan into two 12.9 mm scans. Data from the overlapping 400 µm is present in both new scans.
- Median filter each scan using a length of 5 sample points (equivalent to 5 µm). This removes any outlying data points and effectively acts as a long-pass filter.
- Remove the form by subtracting a first or second-order polynomial fit depending on character of the scan. A linear subtraction was better suited for scans traversed in the spanwise direction. A quadratic subtraction was better suited for scans traversed in the chordwise direction near the leading edge (see Fig. 5).
- Remove waviness using a Gaussian regression filter with a cutoff wavelength (λ_c) of 2.5* mm.
- Remove end effects by cutting 200 µm from the front and back of each 12.9 mm sample to obtain a 12.5* mm evaluation length.
- Divide each evaluation length into five 2.5* mm sampling lengths (L_r).
- Compute R_a (Eq. 2), R_q (Eq. 3), R_{sk} (Eq. 4), R_{ku} (Eq. 5), and the power spectral density (PSD) (Eq. 6) for each sample.

Parameter values denoted by the asterisk (*) are dependent on the computed arithmetic-mean-roughness value, which generally falls within 2.0 µm $< R_a <$ 10.0 µm herein. The dependent values are specified by the ASME B46.1-2002 standard for nonperiodic profiles [9]. A smaller surface roughness would require shorter evaluation and sampling lengths and a shorter cutoff wavelength for proper evaluation.

$$n = \frac{L_r}{\Delta s} \tag{1}$$

$$R_a = \frac{1}{n}\sum_{i=1}^{n} |z(s_i)| \tag{2}$$

$$R_q = \sqrt{\frac{1}{n}\sum_{i=1}^{n} [z(s_i)]^2} \tag{3}$$

$$R_{sk} = \frac{1}{n \cdot (R_q)^3}\sum_{i=1}^{n} [z(s_i)]^3 \tag{4}$$

$$R_{ku} = \frac{1}{n \cdot (R_q)^4} \sum_{i=1}^{n} [z(s_i)]^4 \tag{5}$$

$$\text{PSD} = \frac{\Delta s}{n} |\text{FFT}\,[z(s)]\,|^2, \tag{6}$$

where FFT is the fast Fourier transform.

Computations showed that stationary crossflow wavelengths between 3–5 mm were most unstable. Reducing a sample to $L_r = 2.5$ mm prohibits spectral analysis in the range of interest. See Fig. 6 for sample spectra from the p1LE roughness scans. To assess higher wavelengths, only the second and third items listed in the algorithm above were performed: a form subtraction and median filter. The spectra are the only data reported using this abbreviated method. A comparison between the spectra from the full scans and the roughness scans in p1LE region is given in Fig. 7.

3.2 Step Height

The step height and gap width between the wing and fairing were evaluated for each scan using the following process. This method is a simplified version of the step analysis presented for the BOLT-2 flight vehicle [10].

- Demarcate the bounds for two trendlines: one leading into the step and one moving away from the step. The difference between the end points closest to the step represent the gap width.
- Determine lines of best fit from the segments of data leading into and moving away from the step.
- Extrapolate the lines to the center of the gap and determine the magnitude difference. This value is the step height.
- Determine the location and magnitude of an extreme peak or valley within the gap. The value of this feature is measured relative to the projected trendline that gives the least extreme value.

The elements within these processing steps are summarized in Fig. 8 for a chordwise-directed scan taken across the interface on the starboard wing. The incoming and outgoing bounds were selected by mouse click, so each scan was processed five times to moderate differences based on subjective evaluation. This particular scan has a peak and a valley within the RTV gap between the fairing and wing. Only the peak was quantified in the analysis since it was the most extreme feature.

4 Results

This section summarizes all of the measurements made using the stylus profilometer. Subsection 4.1 details the roughness parameters, and Subsection 4.2 presents the spectra from each region. Finally, Subsection 4.3 evaluates the step height and gap width at the interface between the wing and fairing.

4.1 Roughness Parameters

The roughness parameters (R_a, R_q, R_{sk}, R_{ku}) from all regions of the wings are summarized in Tables 4 – 13. The arithmetic-mean-roughness-height (R_a) statistics for scans performed on the port wing are listed in Table 4 and Table 5 for the quadratic and linear form subtractions, respectively. The statistical values are generally within 1% of each other when considering the different polynomial subtractions for the same scan. The exceptions involve scans made in the chordwise direction near the leading edge, where there is significant curvature, e.g., see Fig. 5. Since the form from the raw scan is not properly removed using a linear subtraction, the range in the waviness profile is significantly higher in Fig. 5(c) than Fig. 5(d). Consequently, less waviness is removed from the roughness profile from which the parameters are computed. Subtracting a linear form, rather than the better-suited quadratic form, results in up to 5% higher R_a values.

The R_a and R_q parameters are further summarized in histograms in Figs. 9 – 16. The R_a values from all scans on the port wings are shown in the histograms in Figs. 9 and 10. The appropriate form subtractions are applied for the histogram plots, a linear subtraction for most regions and a quadratic subtraction for chordwise-directed scans near the leading edge. The bin width is set to a constant 0.1 µm and the height is the probability, i.e., the number of scans within the bin width divided by the total number of scans in the region. The black dashed line shows the median value and the red dashed lines bound 95% of the values. The limits on the R_a axis are held constant to allow for easy comparison between regions; however, there are a few outliers off the scale. The plots clearly show that there are some differences in surface roughness depending on the region that was measured, both in terms of median value and variance. There is generally better agreement between scans of different orientation taken in the same region. Most of the distributions are near normal but slightly skewed to higher R_a values as evidenced by higher mean than median values and by a larger spread between the 50% and 97.5% values in comparison to the spread between the 2.5% and 50% values. This is expected because surface roughness is physically bounded by a minimum value.

Since there are regional differences in the roughness, ranging from R_a median values of 2.27 µm for p1LEc scans to 2.96 µm for p1mid scans, the standard deviation of all scan values on each wing remains high despite the large number of scans. Note that the tabulated standard deviation values were computed by considering all scans together, rather than pooling the standard deviation from each region. However, the standard error of the mean, i.e., the standard deviation normalized by the square root of the total number of samples, suggests that the sample mean is quite close to the population mean, which is the true mean of the regions that were measured.

The mean R_a and R_q for the port wing are 2.512 ± 0.014 µm and 3.104 ± 0.016 µm, respectively, with uncertainty bounds expressed as twice the standard error. The mean R_a and R_q for the starboard wing are 2.870 ± 0.013 µm and 3.532 ± 0.015 µm, respectively.

The higher order statistical moments, skewness (R_{sk}) and kurtosis (R_{ku}), were also computed from the roughness scans and are recorded in Tables 12 and 13. The average skewness value across the regions is near zero, with roughly half the regions having positive and half having negative skewness. This indicates that the roughness distribution favors neither peaks nor valleys. The kurtosis is a measure of the sharpness of the profile peaks. It was remarkably consistent over all regions, ranging from a mean value of 2.61 in two different regions to 2.74 in s2LE. $R_{ku} < 3$ signifies an even, less pronounced surface texture with relatively flat peaks and valleys [11].

4.2 Roughness Spectra

Power spectral density plots were generated to identify dominant wavelengths in the roughness. Figure 6 shows spectra representing the roughness profile sampling length in Fig. 4 and the mean spectra of all sampling lengths in the p1LE region. Note that the PSD values plotted are twice the half spectral values since the PSD is a mirrored function as it is defined herein. The spectra for only a single sampling length are extremely noisy, varying by multiple orders of magnitude over several wavelength increments. However, the spectra show strong agreement regardless of polynomial form subtraction since that mainly effects longer wavelengths. The roughness spectra averaged over the 310 p1LE sampling lengths are much cleaner in appearance, increasing in magnitude with wavelength except for the increment from 1.25 mm to 2.5 mm. Note that these data were processed with a cutoff frequency (λ_c) of 2.5 mm, so the roll off is expected.

With wavelengths between 3–5 mm of greatest significance, the full 25.4 mm scans were evaluated for spectral content. The longer scans have a factor of ten fewer averages, so the spectra have more random noise in comparison to the average of all spectra obtained from the 2.5 mm sampling lengths. A comparison for the same p1LE region is shown in Fig. 7. Note that there are a couple of peaks around the 3–5 mm range, but it is difficult to discern if the variation is greater than expected given the high level of spectral noise and it being within the confidence interval of the PSD.

The effect of the polynomial used in the form subtraction is observed in the spectra from region p1LE in Fig. 17. As previously observed in the spectra from the 2.5 mm sampling lengths (Fig. 6), there is strong agreement between the spectra from the spanwise scans in p1LE for the two different polynomial subtractions. However, spectra from the chordwise scans near the leading edge diverge at the longer wavelengths ($\lambda > 1$) since a linear form subtraction results in considerably higher range in the data.

Spectra from the full 25.4 mm spanwise scans in regions near the leading edge for the port and starboard wings are shown in Figs. 18 and 19, respectively. Periodic roughness from these scans should have the greatest impact on the amplification of

the stationary crossflow instability out of all the orientations and regions measured. The spectra from all three regions on the port wing have considerable peakedness within the 3–5 mm range in comparison to those on the starboard wing. However, the three regions on the port wing also have the three lowest R_a values. The starboard wing includes the repeated region s2LEre. The spectra between the two sets of scans in the same region generally show strong agreement except for a few small peaks. The remaining spectra derived from the full scans are shown in Figs. 20 to 25 for completeness.

The differences in spectra between the wings may provide an explanation for the transition results reported in Leidy et al [6]. For most angles of incidence, the transition front was slightly farther upstream on the starboard wing, which could be attributed to slightly higher average surface roughness. However, as angle of incidence was brought below zero, the transition front on the inboard portion of the port wing was first to advance and in a jagged fashion, consistent with transition due to the stationary crossflow instability. The roughness causing the spectral peaks in the port wing scans may have contributed to crossflow-dominated transition at a less extreme angle of incidence on port wing.

The spectra obtained from the shorter sampling length scans are shown in Figs. 26 to 29. While these spectra do not provide useful content for $\lambda > 1$ mm, they do render PSD values at shorter wavelengths with less random error compared to the full scans. The purpose of these figures is to provide the shape of the spectra at shorter wavelengths and to demonstrate the agreement in that shape between the different regions. The differences in the spectra cannot generally be discerned from these figures for $\lambda < 0.2$ mm.

4.3 Wing/Fairing Interface Characterization

Most scans across the interface between the wing and fairing were taken in the chordwise direction. The sample scan in Fig. 8 demonstrates estimation of the features of interest: the gap width, step height, and peak height. A summary of those parameters for all interface scans is presented in Table 14. The gap width for most scans was between 3–5 mm, but this may be an overestimate since RTV on the top surface of either part is considered part of the gap in the present analysis. The step on both wings was backward facing, meaning both fairings were positioned slightly higher than designed relative to the wings. The step height on both wings also consistently increased in magnitude as distance from the fuselage decreased. For example, a backward-facing step of 291 µm was measured on the port wing near $Y/b = -0.16$, and the step decreased to 41.2 µm near $Y/b = -0.23$.

Only a few scans were taken parallel to the leading edge due to the difficulty in leveling the profilometer. Since the spanwise scans were not taken perpendicular to the interface, the true gap width is actually less than reported when accounting for the wing sweep. Even so, the spanwise directed scans suggest smaller gap widths and step heights on the lateral portion of the interface. However, the flow often tripped downstream of this seam, due to its intersection with the leading edge [6]. The measured steps from the lateral scans indicate that the fairing was slightly higher than the wing on the port side, and the wing was slightly higher than the

fairing on the starboard side.

5 Summary

Surface roughness measurements were made on the NASA Juncture Flow model wings prior to the 2022 entry in the NASA Langley 14- by 22-Foot Subsonic Tunnel. Measurements were acquired using a stylus profilometer at six different regions on each wing, with scans directed in the spanwise and chordwise directions. Roughness parameters from the scans were evaluated in accordance with the ASME B46.1-2002 standards. Additionally, full length scans were analyzed for longer wavelength content that was computationally shown to amplify the stationary crossflow instability. The roughness levels were higher on the starboard wing ($R_q = 3.532 \pm 0.015$ µm) compared to the port wing ($R_q = 3.104 \pm 0.016$ µm). However, the PSD plots from scans on the port wing indicate more peaks present for wavelengths between 3–5 mm. These findings are consistent with the transition results reported from the campaign. Additionally, profilometer scans were made with the model fully assembled within the tunnel at the wing/fairing interface on both wings. These scans indicate backward-facing steps that decreased in height farther outboard along the interface.

References

1. Rumsey, C. L., "NASA Langley Turbulence Modeling Resource Website," https://turbmodels.larc.nasa.gov.

2. Kegerise, M. A. and Neuhart, D. H., "An Experimental Investigation of a Wing-Fuselage Junction Model in the NASA Langley 14- by 22-Foot Subsonic Tunnel," NASA/TM-2019-220286, June 2019. https://doi.org/2060/20190027403

3. Kegerise, M. A., Neuhart, D. H., Hannon, J. A., Rumsey, C. L., "An Experimental Investigation of a Wing-Fuselage Junction Model in the NASA Langley 14- by 22-Foot Subsonic Wind Tunnel," AIAA SciTech Forum, AIAA Paper 2019-0077, January 2019. https://doi.org/10.2514/6.2019-0077

4. Jenkins, L. N., Yao, C.-S., Bartram, S. M., "Flow-Field Measurements in a Wing-Fuselage Junction Using an Embedded Particle Image Velocimetry System," AIAA SciTech Forum, AIAA Paper 2019-0078, January 2019. https://doi.org/10.2514/6.2019-0078

5. Rumsey, C. L., Ahmad, N. N., Carlson, J.-R., Kegerise, M. A., Neuhart, D. H., Hannon, J. A., Jenkins, L. N., Yao, C.-S., Balakumar, P., Gildersleeve, S., Bartram, S. M., Pulliam, T. H., Olsen, M. E., and Spalart, P. R., "NASA Juncture Flow Computational Fluid Dynamics Validation Experiment," *AIAA Journal*, Vol. 60, No. 8, 2022, pp. 4789-4805. https://doi.org/10.2514/1.J061600

6. Leidy, A. N., Kegerise, M. A., Hannon, J., Choudhari, M. M., Venkatachari, B. S., and Paredes, P., "Measurements and Computations of Natural Transition on the NASA Juncture-Flow Model with a Symmetric Wing," AIAA SciTech Forum, AIAA Paper 2023-0441, January 2023. https://doi.org/10.2514/6.2023-0441

7. Kegerise, M. A., Leidy, A. N., Hannon, J., Rumsey, C. L., "Measurements and Computational Analysis of the Turbulent Corner Flow on the NASA Juncture-Flow Model with a Symmetric Wing," NASA/TP-20240004000, April 2024. https://doi.org/2060/20240004000

8. Kegerise, M. A., Leidy, A. N., Hannon, J., Rumsey, C. L., and Pulliam, T. H., "Measurements and Computations of the Turbulent Corner Flow on the NASA Juncture-Flow Model with a Symmetric Wing," AIAA SciTech Forum, AIAA Paper 2023-0440, January 2023. https://doi.org/10.2514/6.2023-0440

9. *Surface Texture (Surface Roughness, Waviness, and Lay): An American National Standard*, ASME B46.1-2002, The American Society of Mechanical Engineers, New York, 2003.

10. Leidy, A., "BOLT-2 Forebody Surface Measurement Analysis," NASA/TM-20230000169, January 2023. https://doi.org/2060/20230000169

11. Gadelmawla, E. S., Koura, M. M., Maksoud, T. M. A., Elewa, I. M., and Soliman, H.H., "Roughness parameters," *Journal of Materials Processing Technology*, Vol. 123, No. 1, 2002, pp. 133-145. https://doi.org/10.1016/S0924-0136(02)00060-2

Table 1: Scan regions on port wing.

Name	Direction	Scans	x'/c	$(-)Y/b$
p1LE	spanwise	31	0.050–0.062	0.83–0.87
p1LEc	chordwise	42	0.059–0.12	0.84–0.87
p1mid	spanwise	33	0.45–0.55	0.82–0.87
p1midc	chordwise	37	0.39–0.48	0.80–0.83
p2LE	spanwise	35	0.038–0.055	0.60–0.64
p2LEc	chordwise	31	0.061–0.11	0.61–0.63
p2mid	spanwise	30	0.45–0.55	0.57–0.61
p2midc	chordwise	33	0.42–0.50	0.57–0.60
p3LE	spanwise	33	0.038–0.072	0.44–0.49
p3LEc	chordwise	34	0.062–0.11	0.46–0.48
p3mid	spanwise	35	0.45–0.55	0.41–0.46
p3midc	chordwise	42	0.44–0.52	0.43–0.46

Table 2: Scan regions on starboard wing.

Name	Direction	Scans	x'/c	Y/b
s1LE	spanwise	33	0.090–0.11	0.82–0.87
s1LEc	chordwise	32	0.095–0.16	0.84–0.87
s1mid	spanwise	35	0.45–0.55	0.82–0.87
s1midc	chordwise	34	0.46–0.56	0.83–0.86
s2LE	spanwise	37	0.044–0.060	0.60–0.64
s2LEre	spanwise	31	0.047–0.062	0.60–0.64
s2LEc	chordwise	30	0.075–0.13	0.61–0.63
s2mid	spanwise	32	0.45–0.55	0.60–0.64
s2midc	chordwise	38	0.46–0.55	0.60–0.63
s3LE	spanwise	41	0.046–0.074	0.44–0.49
s3LEc	chordwise	38	0.063–0.11	0.46–0.48
s3mid	spanwise	35	0.45–0.55	0.44–0.49
s3midc	chordwise	33	0.44–0.52	0.45–0.48

Table 3: Wing/fairing interface scan locations.

Name	Direction	Scans	X (m)	Y/b
pi	chordwise	22	across 2.234	-(0.16–0.23)
pil	spanwise	2	2.23	across -0.230
si	chordwise	22	across 2.234	0.16–0.23
sil	spanwise	1	2.23	across 0.230

Table 4: Measured R_a on the port wing. Scans were processed using a quadratic-fit subtraction.

Name	Scans	R_a (µm)						
		Min	25%	Med	75%	Max	Mean	Stdev
p1LE	310	1.57	2.09	2.29	2.52	3.33	2.32	0.318
p1LEc	420	1.57	2.07	2.27	2.47	3.76	2.30	0.316
p1mid	330	1.74	2.67	2.96	3.39	4.49	3.02	0.491
p1midc	370	1.67	2.40	2.68	3.05	4.37	2.74	0.465
p2LE	350	1.54	2.08	2.32	2.56	3.49	2.33	0.341
p2LEc	310	1.58	2.38	2.63	2.94	4.19	2.66	0.431
p2mid	300	1.66	2.15	2.41	2.64	6.78	2.43	0.442
p2midc	330	1.67	2.20	2.40	2.70	3.78	2.46	0.374
p3LE	330	1.66	2.26	2.50	2.80	3.69	2.55	0.394
p3LEc	340	1.76	2.31	2.53	2.80	3.98	2.56	0.465
p3mid	350	1.70	2.20	2.41	2.60	4.66	2.43	0.351
p3midc	420	1.64	2.18	2.37	2.59	5.33	2.40	0.361
All port	4160	1.54	2.21	2.45	2.76	6.78	2.51	0.438

Table 5: Measured R_a on the port wing. Scans were processed using a linear-fit subtraction.

Name	Scans	R_a (µm)						
		Min	25%	Med	75%	Max	Mean	Stdev
p1LE	310	1.57	2.10	2.29	2.52	3.33	2.32	0.316
p1LEc	420	1.57	2.16	2.36	2.59	3.76	2.39	0.345
p1mid	330	1.74	2.67	2.96	3.39	4.49	3.02	0.492
p1midc	370	1.67	2.41	2.68	3.06	4.37	2.74	0.465
p2LE	350	1.54	2.08	2.32	2.56	3.49	2.33	0.339
p2LEc	310	1.73	2.41	2.70	3.06	4.19	2.73	0.460
p2mid	300	1.66	2.15	2.41	2.64	6.78	2.45	0.442
p2midc	330	1.67	2.20	2.40	2.70	3.78	2.46	0.375
p3LE	330	1.66	2.25	2.50	2.80	3.70	2.54	0.394
p3LEc	340	1.64	2.35	2.57	2.85	4.05	2.60	0.378
p3mid	350	1.70	2.21	2.41	2.60	4.66	2.43	0.351
p3midc	420	1.64	2.18	2.37	2.59	5.33	2.40	0.361
All port	4160	1.54	2.22	2.47	2.77	6.78	2.53	0.441

Table 6: Measured R_a on the starboard wing. Scans were processed using a quadratic-fit subtraction.

Name	Scans	R_a (µm)						
		Min	25%	Med	75%	Max	Mean	Stdev
s1LE	330	1.72	2.61	2.91	3.19	3.96	2.92	0.418
s1LEc	320	1.84	2.62	2.91	3.30	4.42	2.97	0.462
s1mid	350	1.97	2.49	2.71	3.01	4.05	2.76	0.378
s1midc	340	1.89	2.42	2.66	2.88	4.43	2.70	0.363
s2LE	370	1.88	2.43	2.69	2.96	3.91	2.72	0.382
s2LEre	310	1.85	2.50	2.77	3.11	3.98	2.82	0.437
s2LEc	300	1.93	2.58	2.84	3.12	4.17	2.88	0.409
s2mid	320	1.72	2.74	2.99	3.30	4.76	3.02	0.425
s2midc	380	2.07	2.71	3.01	3.33	4.65	3.04	0.444
s3LE	410	1.79	2.35	2.64	2.91	4.22	2.65	0.417
s3LEc	380	1.86	2.61	2.89	3.19	4.22	2.91	0.417
s3mid	350	1.98	2.68	2.95	3.25	5.65	2.99	0.439
s3midc	330	1.75	2.72	2.99	3.28	4.34	2.99	0.416
All star.	4490	1.72	2.56	2.83	3.15	5.65	2.87	0.436

Table 7: Measured R_a on the starboard wing. Scans were processed using a linear-fit subtraction.

Name	Scans	R_a (µm)						
		Min	25%	Med	75%	Max	Mean	Stdev
s1LE	330	1.72	2.61	2.90	3.19	3.97	2.92	0.418
s1LEc	320	2.04	2.65	2.95	3.34	4.56	3.01	0.474
s1mid	350	1.97	2.49	2.71	3.01	4.05	2.76	0.378
s1midc	340	1.92	2.43	2.67	2.87	4.47	2.70	0.364
s2LE	370	1.89	2.44	2.69	2.96	3.91	2.72	0.383
s2LEre	310	1.82	2.50	2.77	3.11	3.98	2.82	0.438
s2LEc	300	1.93	2.64	2.89	3.16	4.17	2.92	0.409
s2mid	320	1.72	2.74	2.99	3.31	4.76	3.02	0.425
s2midc	380	2.07	2.71	3.01	3.34	4.65	3.04	0.444
s3LE	410	1.79	2.35	2.63	2.90	4.22	2.65	0.417
s3LEc	380	1.86	2.67	2.93	3.25	4.22	2.97	0.429
s3mid	350	1.98	2.68	2.95	3.25	5.65	2.99	0.439
s3midc	330	1.75	2.72	2.99	3.27	4.34	2.99	0.416
All star.	4490	1.72	2.57	2.84	3.17	5.65	2.88	0.440

Table 8: Measured R_q on the port wing. Scans were processed using a quadratic-fit subtraction.

Name	Scans	R_q (µm)						
		Min	25%	Med	75%	Max	Mean	Stdev
p1LE	310	1.99	2.60	2.81	3.09	3.95	2.86	0.376
p1LEc	420	1.96	2.58	2.82	3.05	4.53	2.85	0.379
p1mid	330	2.27	3.30	3.63	4.13	5.25	3.71	0.567
p1midc	370	2.04	3.02	3.34	3.71	5.67	3.39	0.544
p2LE	350	1.96	2.57	2.86	3.12	4.02	2.87	0.400
p2LEc	310	2.04	2.96	3.27	3.61	4.92	3.29	0.496
p2mid	300	2.06	2.68	3.02	3.25	9.19	3.03	0.567
p2midc	330	2.11	2.73	3.01	3.33	4.71	3.04	0.440
p3LE	330	2.11	2.82	3.10	3.41	4.40	3.14	0.465
p3LEc	340	2.27	2.85	3.11	3.39	4.87	3.15	0.430
p3mid	350	2.11	2.75	2.97	3.25	7.22	3.02	0.452
p3midc	420	2.06	2.71	2.91	3.22	8.00	2.97	0.460
All port	4160	1.96	2.75	3.04	3.38	9.19	3.10	0.525

Table 9: Measured R_q on the port wing. Scans were processed using a linear-fit subtraction.

Name	Scans	R_q (µm)						
		Min	25%	Med	75%	Max	Mean	Stdev
p1LE	310	1.99	2.60	2.81	3.09	3.95	2.86	0.374
p1LEc	420	1.97	2.69	2.94	3.21	5.00	2.97	0.416
p1mid	330	2.26	3.30	3.63	4.13	5.25	3.71	0.567
p1midc	370	2.04	3.02	3.36	3.71	5.67	3.39	0.545
p2LE	350	1.96	2.57	2.86	3.13	4.02	2.87	0.399
p2LEc	310	2.16	2.99	3.35	3.73	4.92	3.38	0.533
p2mid	300	2.06	2.68	3.02	3.25	9.19	3.03	0.566
p2midc	330	2.11	2.74	3.01	3.33	4.71	3.05	0.441
p3LE	330	2.12	2.82	3.10	3.42	4.40	3.14	0.465
p3LEc	340	2.09	2.90	3.17	3.48	4.95	3.20	0.440
p3mid	350	2.11	2.75	2.97	3.25	7.22	3.02	0.452
p3midc	420	2.06	2.71	2.91	3.22	8.00	2.97	0.461
All port	4160	1.96	2.77	3.06	3.41	9.19	3.13	0.530

Table 10: Measured R_q on the starboard wing. Scans were processed using a quadratic-fit subtraction.

Name	Scans	R_q (µm)						
		Min	25%	Med	75%	Max	Mean	Stdev
s1LE	330	2.22	3.25	3.58	3.91	5.39	3.60	0.487
s1LEc	320	2.26	3.24	3.59	4.04	5.40	3.65	0.550
s1mid	350	2.41	3.08	3.36	3.68	4.86	3.40	0.440
s1midc	340	2.42	3.03	3.29	3.56	5.16	3.33	0.423
s2LE	370	2.37	3.03	3.31	3.64	4.84	3.36	0.457
s2LEre	310	2.26	3.12	3.41	3.82	4.84	3.47	0.509
s2LEc	300	2.50	3.20	3.51	3.86	4.94	3.55	0.478
s2mid	320	2.24	3.36	3.67	4.00	5.64	3.71	0.503
s2midc	380	2.52	3.35	3.70	4.07	5.41	3.72	0.511
s3LE	410	2.22	2.93	3.25	3.57	5.12	3.27	0.488
s3LEc	380	2.31	3.24	3.58	3.90	5.08	3.59	0.487
s3mid	350	2.45	3.29	3.66	3.98	7.76	3.67	0.527
s3midc	330	2.20	3.36	3.68	4.00	5.18	3.67	0.483
All star.	4490	2.20	3.17	3.50	3.86	7.76	3.53	0.511

Table 11: Measured R_q on the starboard wing. Scans were processed using a linear-fit subtraction.

Name	Scans	R_q (µm)						
		Min	25%	Med	75%	Max	Mean	Stdev
s1LE	330	2.23	3.26	3.58	3.90	5.39	3.60	0.487
s1LEc	320	2.47	3.31	3.65	4.11	5.60	3.71	0.566
s1mid	350	2.41	3.09	3.36	3.69	4.86	3.40	0.440
s1midc	340	2.43	3.03	3.30	3.56	5.19	3.33	0.423
s2LE	370	2.37	3.03	3.31	3.64	4.84	3.36	0.458
s2LEre	310	2.24	3.12	3.41	3.83	4.84	3.47	0.509
s2LEc	300	2.51	3.25	3.58	3.91	4.94	3.60	0.477
s2mid	320	2.24	3.36	3.67	4.00	5.64	3.71	0.503
s2midc	380	2.52	3.34	3.70	4.07	5.41	3.72	0.512
s3LE	410	2.23	2.93	3.25	3.57	5.12	3.27	0.489
s3LEc	380	2.31	3.28	3.65	3.96	5.15	3.66	0.502
s3mid	350	2.45	3.28	3.65	3.98	7.76	3.67	0.527
s3midc	330	2.20	3.35	3.68	4.00	5.18	3.67	0.483
All star.	4490	2.20	3.19	3.51	3.88	7.76	3.55	0.516

Table 12: Measured R_{sk} and R_{ku} on the port wing. Most scans were processed using a linear-fit subtraction. Only chordwise scans near the leading edge were processed using a quadratic-fit subtraction.

Name	Scans	R_{sk}		R_{ku}	
		Mean	Stdev	Mean	Stdev
p1LE	310	0.05	0.27	2.67	0.39
p1LEc	420	0.11	0.30	2.78	0.43
p1mid	330	0.32	0.30	2.68	0.51
p1midc	370	0.32	0.31	2.79	0.55
p2LE	350	-0.10	0.29	2.69	0.42
p2LEc	310	-0.06	0.30	2.70	0.42
p2mid	300	0.01	0.30	2.72	0.42
p2midc	330	0.01	0.30	2.73	0.45
p3LE	330	-0.06	0.31	2.71	0.44
p3LEc	340	-0.01	0.30	2.69	0.43
p3mid	350	0.09	0.30	2.81	0.51
p3midc	420	0.08	0.30	2.74	0.46
All port	4160	0.07	0.33	2.73	0.46

Table 13: Measured R_{sk} and R_{ku} on the starboard wing. Most scans were processed using a linear-fit subtraction. Only chordwise scans near the leading edge were processed using a quadratic-fit subtraction.

Name	Scans	R_{sk}		R_{ku}	
		Mean	Stdev	Mean	Stdev
s1LE	330	0.16	0.31	2.70	0.49
s1LEc	320	0.21	0.31	2.69	0.42
s1mid	350	0.03	0.29	2.70	0.41
s1midc	340	-0.01	0.29	2.69	0.40
s2LE	370	-0.05	0.34	2.74	0.56
s2LEre	310	-0.03	0.30	2.68	0.41
s2LEc	300	-0.03	0.31	2.68	0.46
s2mid	320	0.10	0.30	2.61	0.46
s2midc	380	0.19	0.30	2.62	0.44
s3LE	410	-0.05	0.29	2.73	0.47
s3LEc	380	-0.06	0.31	2.70	0.43
s3mid	350	0.11	0.34	2.67	0.50
s3midc	330	0.14	0.30	2.61	0.40
All star.	4490	0.05	0.32	2.68	0.46

Table 14: Measured parameters at the wing/fairing interface.

Name	Scans	Gap Width (mm)			Step Height (µm)			Peak Height (µm)		
		Min	Med	Max	Min	Med	Max	Min	Med	Max
pi	22	2.77	4.13	4.94	-41.2	-179	-291	1.52	33.2	87.9
pil	2	2.63	3.21	3.80	-41.8	-45.9	-50.0	-82.2	-87.2	-92.2
si	22	2.25	3.18	3.94	-26.2	-144	-223	13.3	61.7	91.0
sil	1	1.38	1.38	1.38	13.1	13.1	13.1	57.6	57.6	57.6

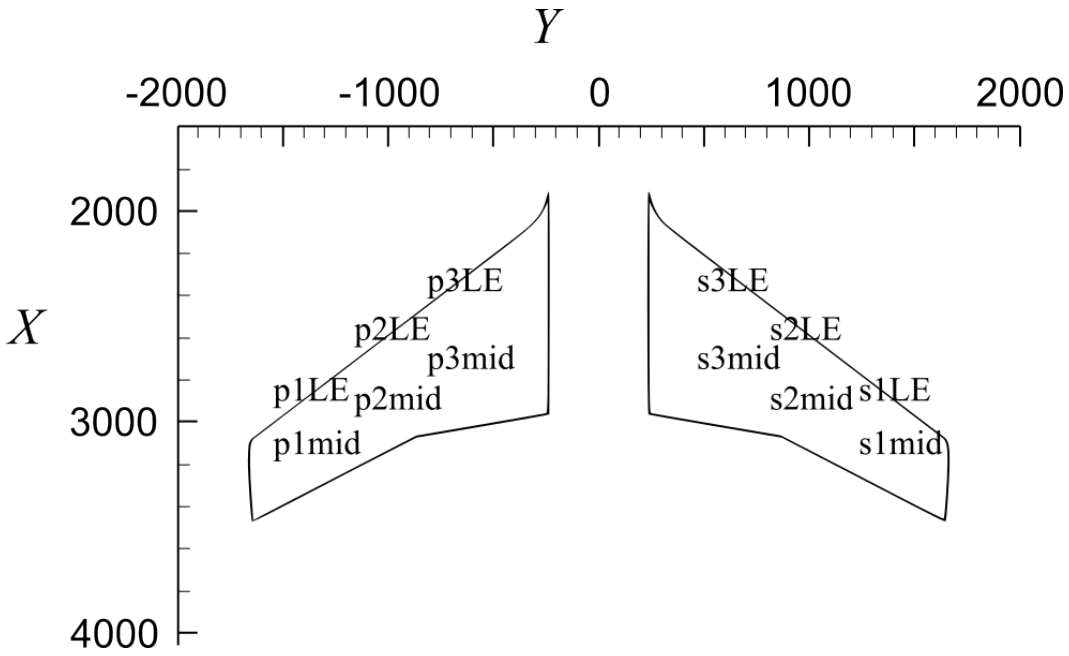

Figure 1: Top view of model wing geometry with regions of surface roughness measurements on the port (p) and starboard (s) sides. Measurements were made near the leading edge (LE) and near mid chord (mid). Model-based coordinates are expressed in mm.

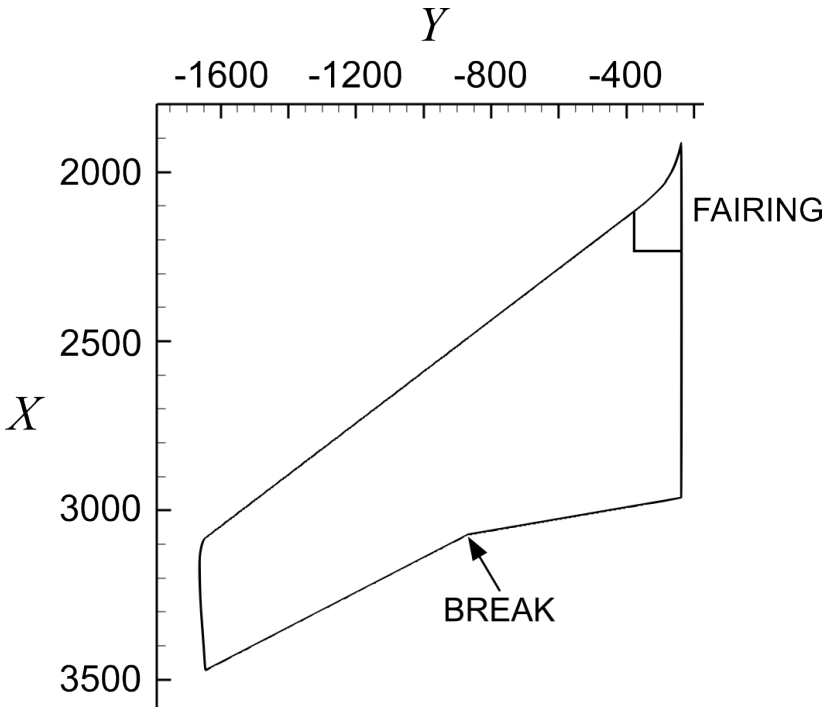

Figure 2: Top view of the wing on the port side of the model. The fairing merges the fuselage and wing geometries to mitigate the adverse pressure gradient at the junction. The gaps between the fairing and wing were filled with RTV silicone and quantified following assembly. Model-based coordinates are expressed in mm.

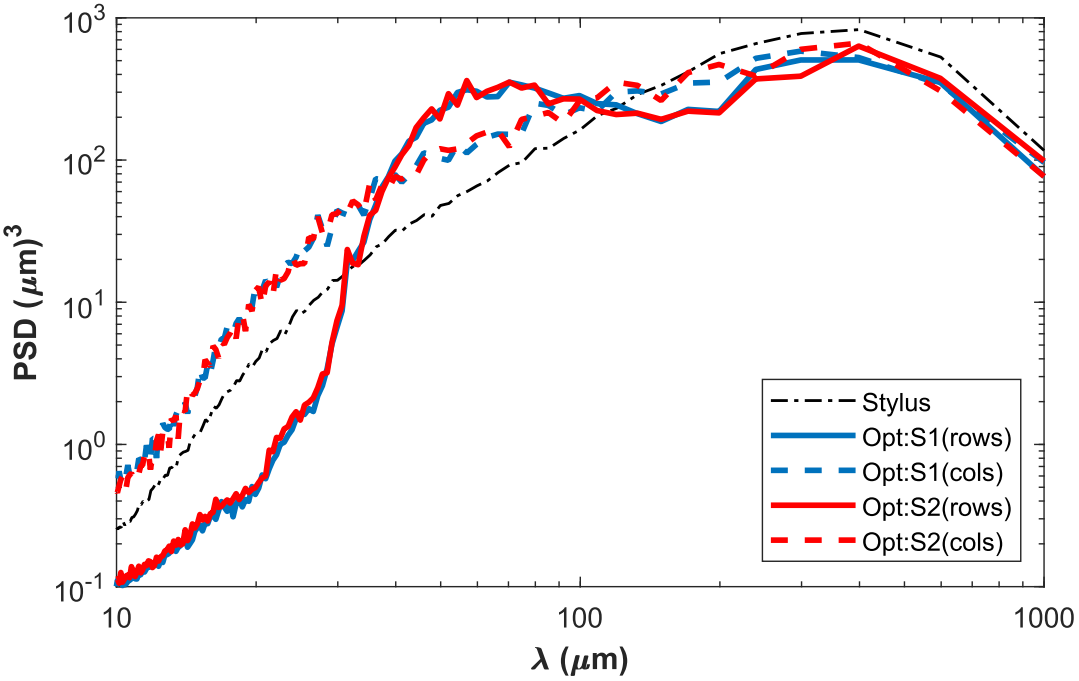

Figure 3: Comparison scans on hatch

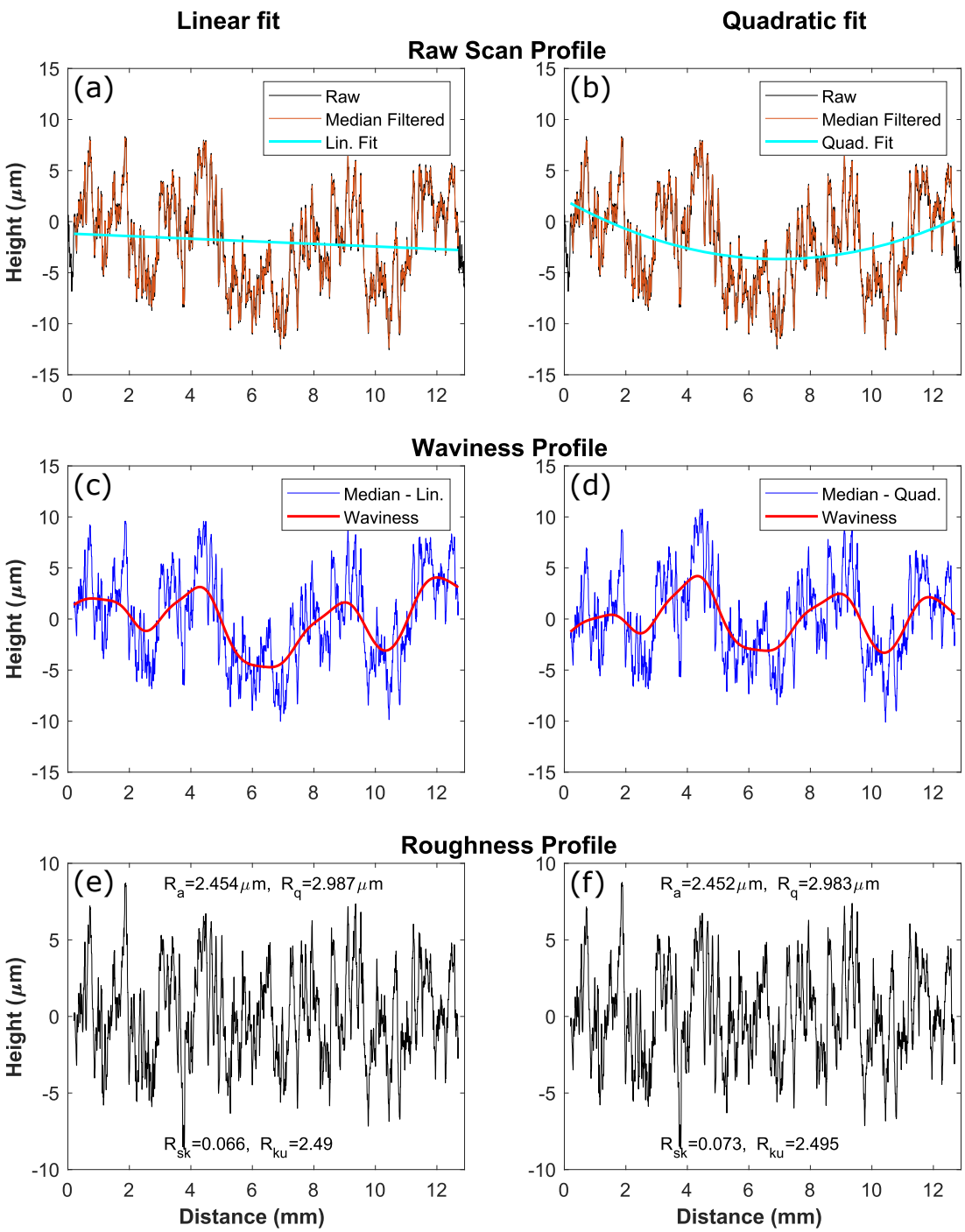

Figure 4: Steps for processing roughness from a sample spanwise scan in the p1LE region. Processing with a linear form fit is shown on the left, and a quadratic fit is on the right. (a) raw, median-filtered, and linear fit of median-filtered profile (b) raw, median-filtered, and quadratic fit of median-filtered profile (c) profile of median-filtered minus linear fit and corresponding waviness profile using $\lambda_c = 2.5$ mm (d) profile of median-filtered minus quadratic fit and corresponding waviness profile using $\lambda_c = 2.5$ mm. (e) roughness profile propagated from the linear data fit (f) roughness profile propagated from the quadratic data fit.

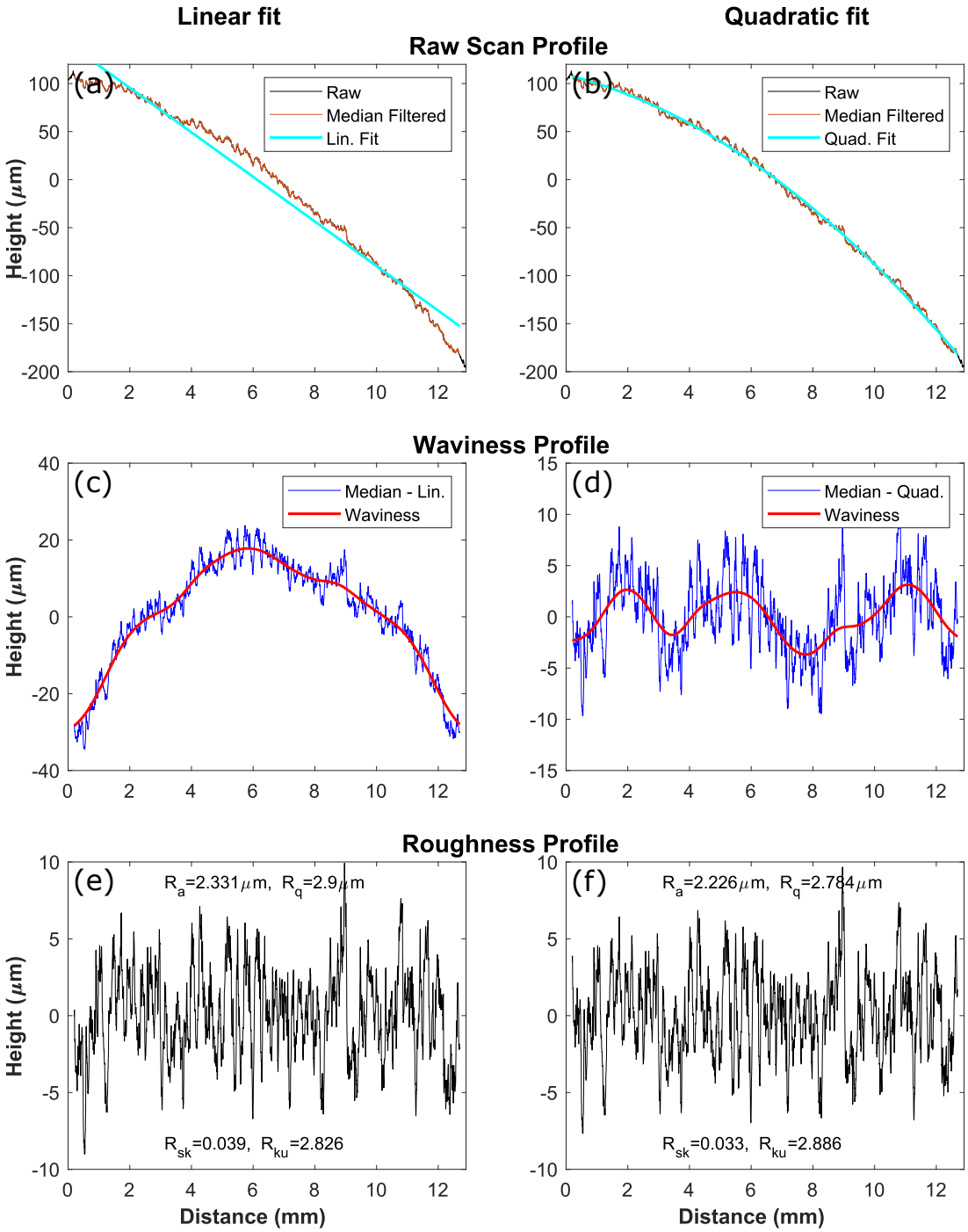

Figure 5: Steps for processing roughness from a sample chordwise scan in the p1LE region. Processing with a linear form fit is shown on the left, and a quadratic fit is on the right. (a) raw, median-filtered, and linear fit of median-filtered profile (b) raw, median-filtered, and quadratic fit of median-filtered profile (c) profile of median-filtered minus linear fit and corresponding waviness profile using $\lambda_c = 2.5$ mm (d) profile of median-filtered minus quadratic fit and corresponding waviness profile using $\lambda_c = 2.5$ mm. (e) roughness profile propagated from the linear data fit (f) roughness profile propagated from the quadratic data fit.

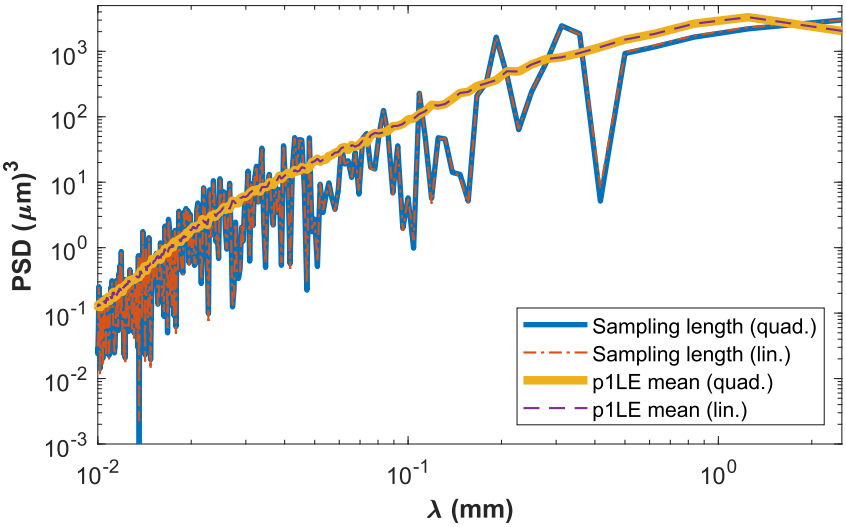

Figure 6: Power spectral density plots featuring different polynomial form subtractions. The "sampling length" PSDs are derived from the final 2.5 mm in the roughness profiles presented in Figs. 4(e) and 4(f). The "p1LE mean" spectra are the average PSD values over 310 sampling lengths in the p1LE scan region. Note the agreement in values between the quadratic and linear subtraction derived spectra for wavelengths up to 2.5 mm.

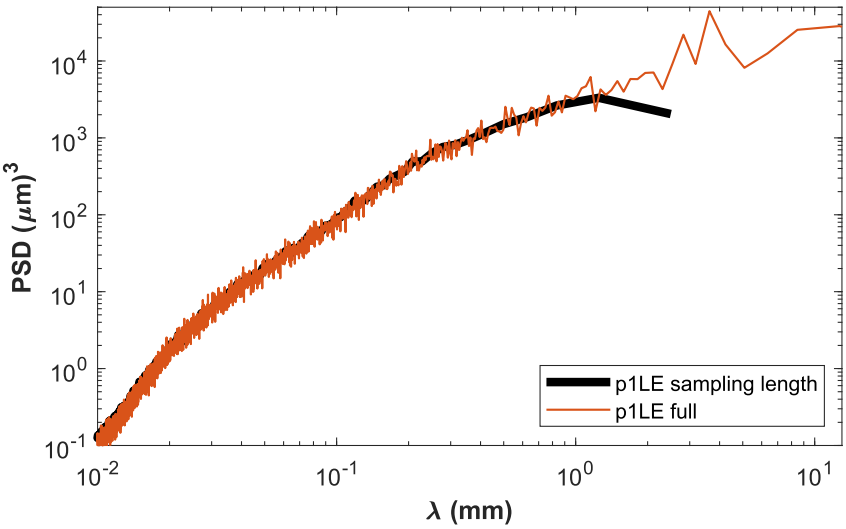

Figure 7: Comparison between the mean sampling length and mean full PSD plots from scans in the p1LE region. The sampling length PSD was generated from 310 $\times$ 2.5 mm sampling lengths and the mean full PSD from 31 $\times$ 25.4 mm full scans. The profiles used to derive the full PSD were median filtered and quadratic form subtracted. Longer scan lengths allow for observation of longer spectral features. There is strong agreement between the sampling length and full spectra for $\lambda < 1$ mm. Effects of the waviness cutoff (λ_c) are observed for for $\lambda > 1$ mm.

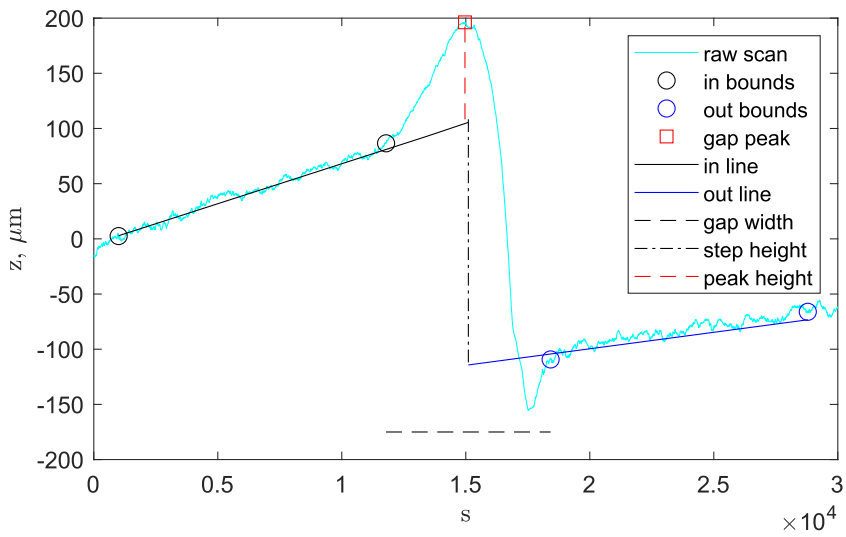

Figure 8: Sample scan of the wing/fairing interface and elements for determining the gap features.

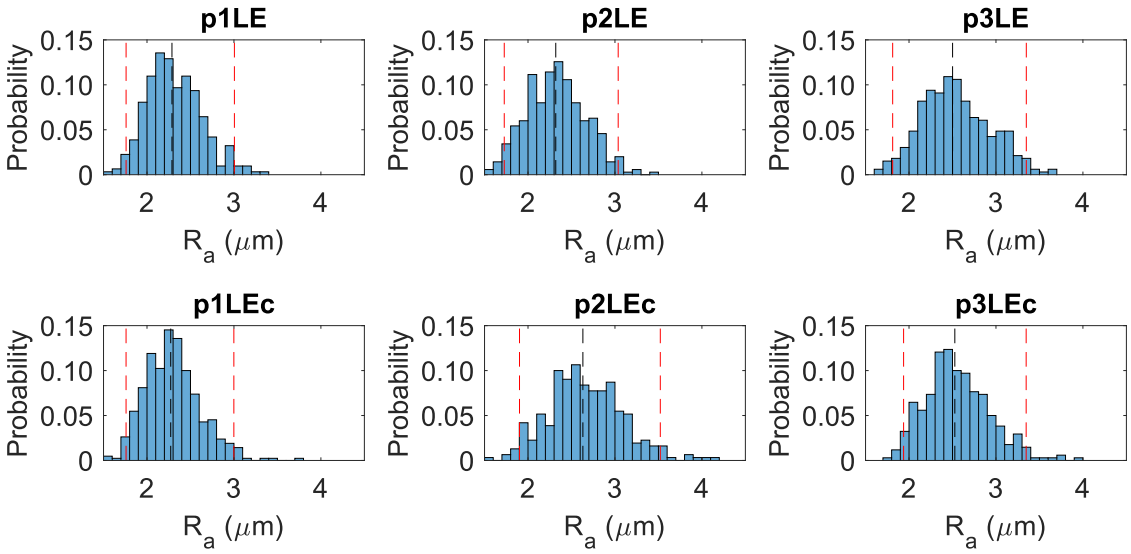

Figure 9: Histograms of R_a values on the port wing in regions near the leading edge. Spanwise scans were processed using a linear-fit subtraction, and chordwise scans were processed using a quadratic-fit subtraction. The black dashed line specifies the median value. The red dashed lines bound 95% of values.

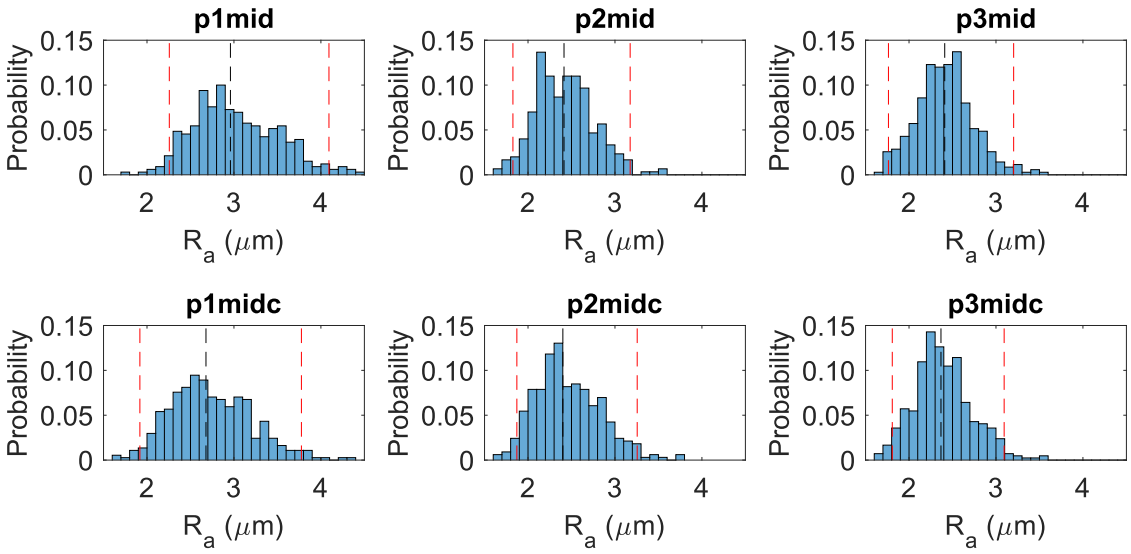

Figure 10: Histograms of R_a values on the port wing in regions near the middle of the chord. Scans were processed using a linear-fit subtraction. The black dashed line specifies the median value. The red dashed lines bound 95% of values.

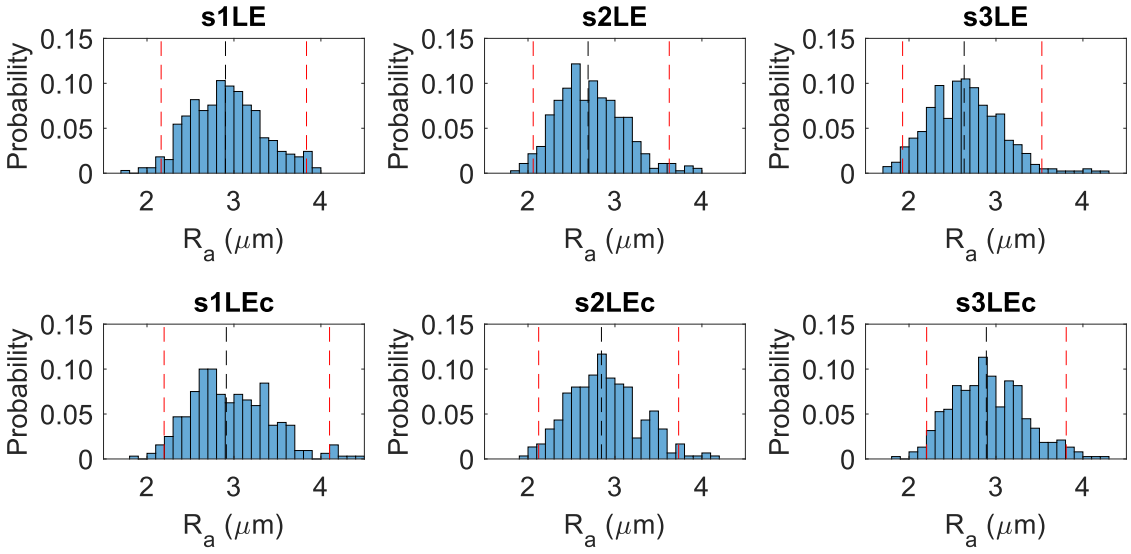

Figure 11: Histograms of R_a values on the starboard wing in regions near the leading edge. Spanwise scans were processed using a linear-fit subtraction, and chordwise scans were processed using a quadratic-fit subtraction. The black dashed line specifies the median value. The red dashed lines bound 95% of values.

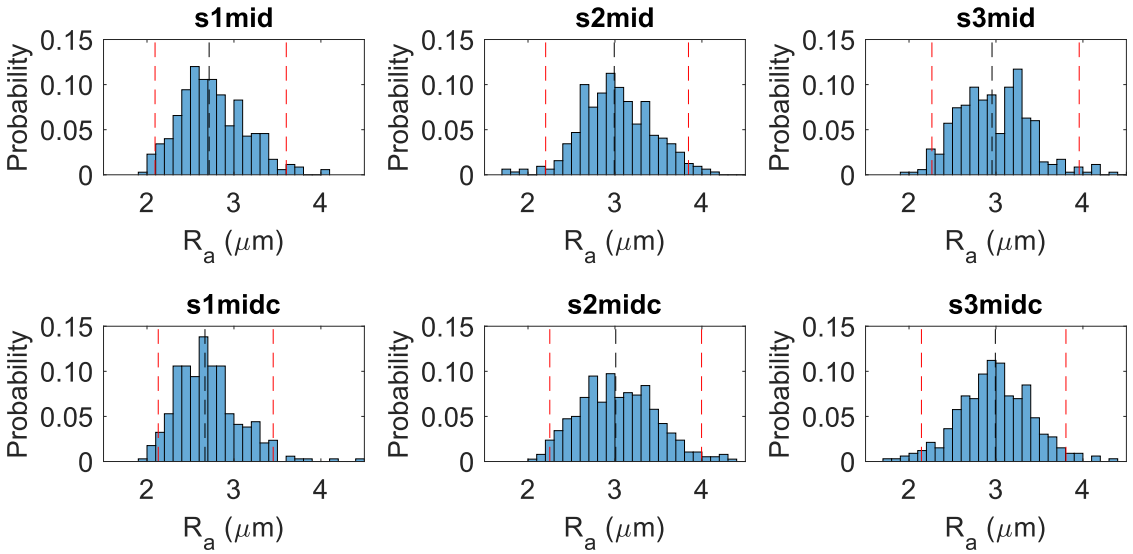

Figure 12: Histograms of R_a values on the starboard wing in regions near the middle of the chord. Scans were processed using a linear-fit subtraction. The black dashed line specifies the median value. The red dashed lines bound 95% of values.

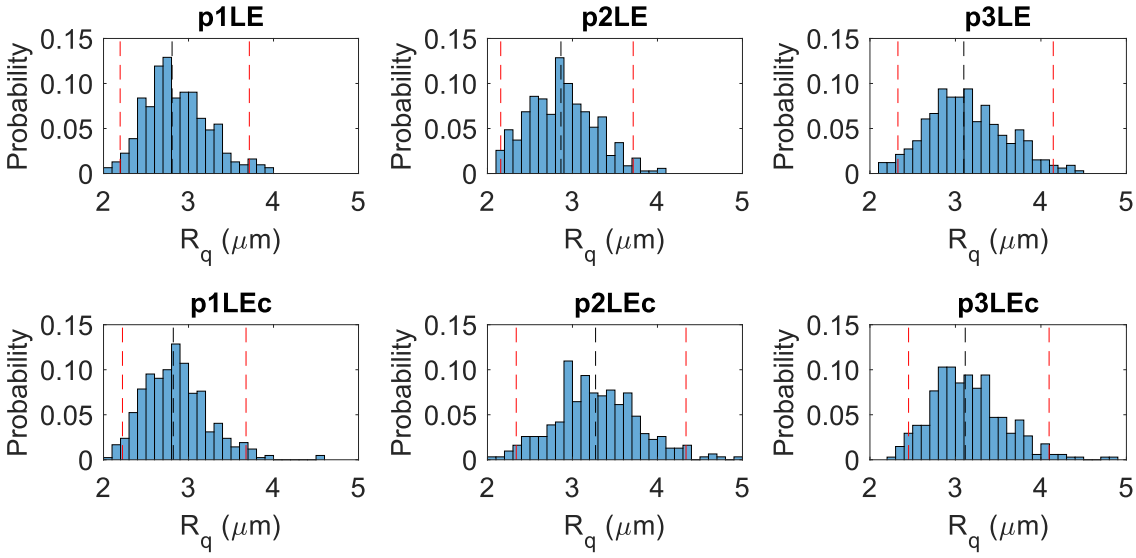

Figure 13: Histograms of R_q values on the port wing in regions near the leading edge. Spanwise scans were processed using a linear-fit subtraction, and chordwise scans were processed using a quadratic-fit subtraction. The black dashed line specifies the median value. The red dashed lines bound 95% of values.

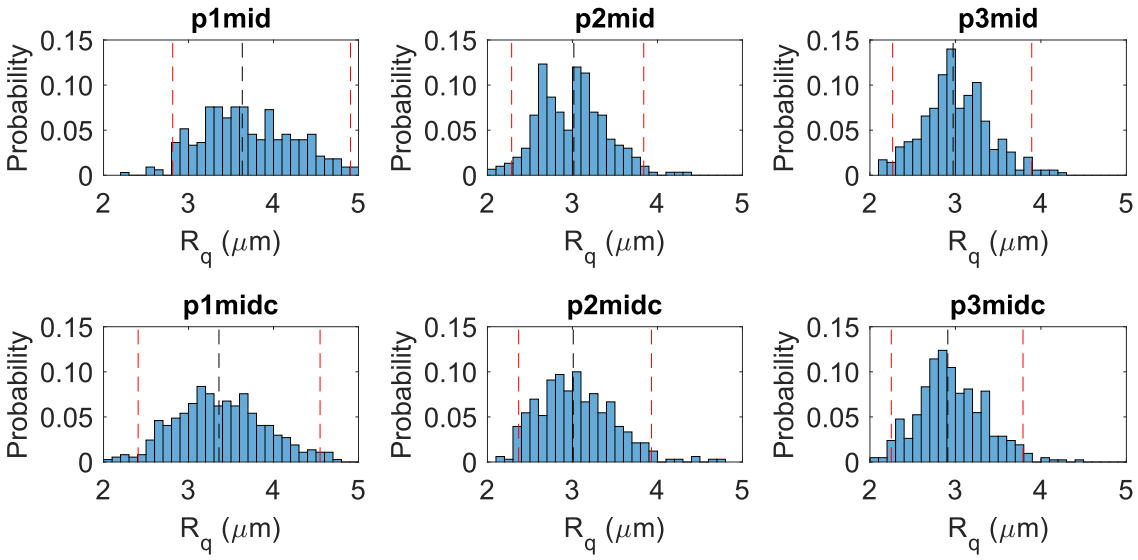

Figure 14: Histograms of R_q values on the port wing in regions near the middle of the chord. Scans were processed using a linear-fit subtraction. The black dashed line specifies the median value. The red dashed lines bound 95% of values.

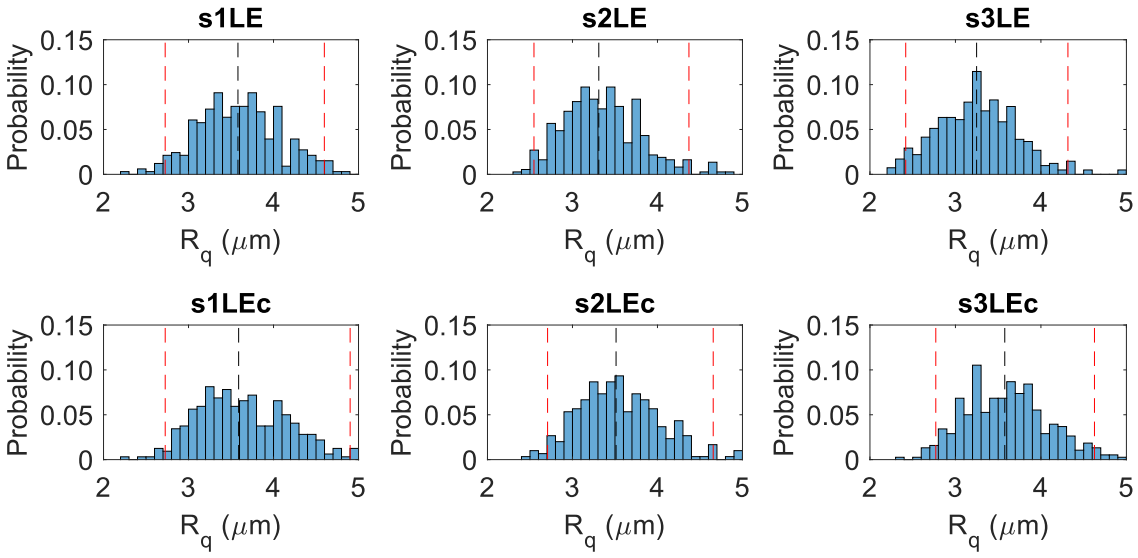

Figure 15: Histograms of R_q values on the starboard wing in regions near the leading edge. Spanwise scans were processed using a linear-fit subtraction, and chordwise scans were processed using a quadratic-fit subtraction. The black dashed line specifies the median value. The red dashed lines bound 95% of values.

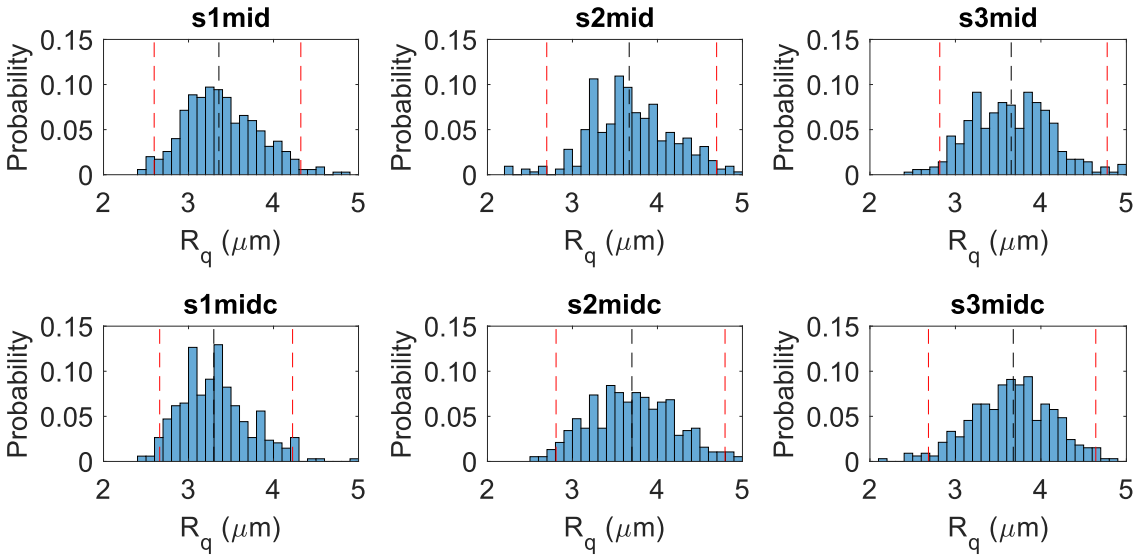

Figure 16: Histograms of R_q values on the starboard wing in regions near the middle of the chord. Scans were processed using a linear-fit subtraction. The black dashed line specifies the median value. The red dashed lines bound 95% of values.

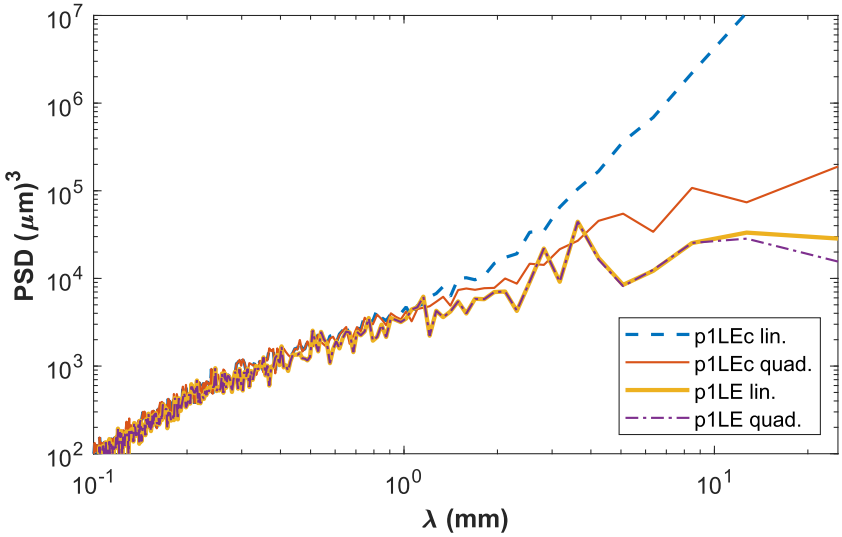

Figure 17: PSD comparison for full scans performed in the chordwise and spanwise directions with linear and quadratic form subtractions. The spectra represent 42 chordwise p1LEc scans and 31 spanwise p1LE scans. The raw chordwise scans include significant model surface curvature, necessitating a quadratic-form subtraction to identify potential wavelength peaks between 1.0–10.0 mm.

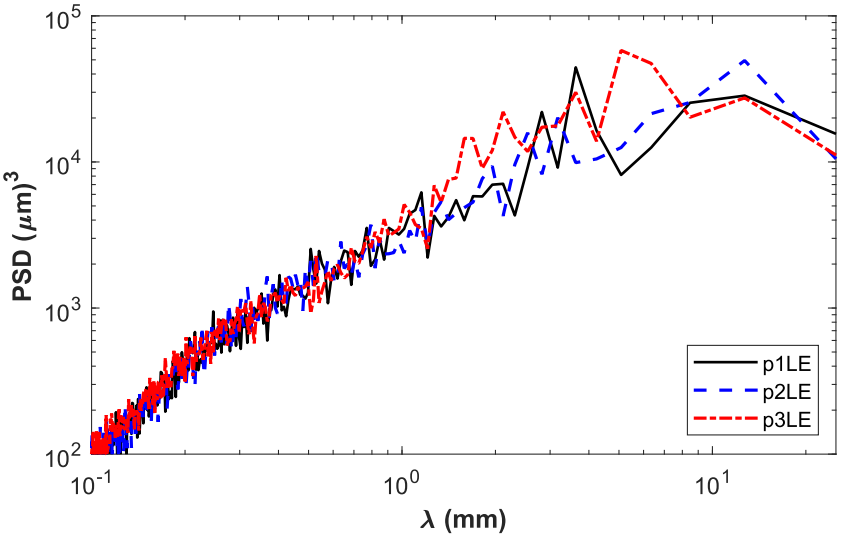

Figure 18: PSD comparison for full scans performed on the port wing near the leading edge and in the spanwise direction.

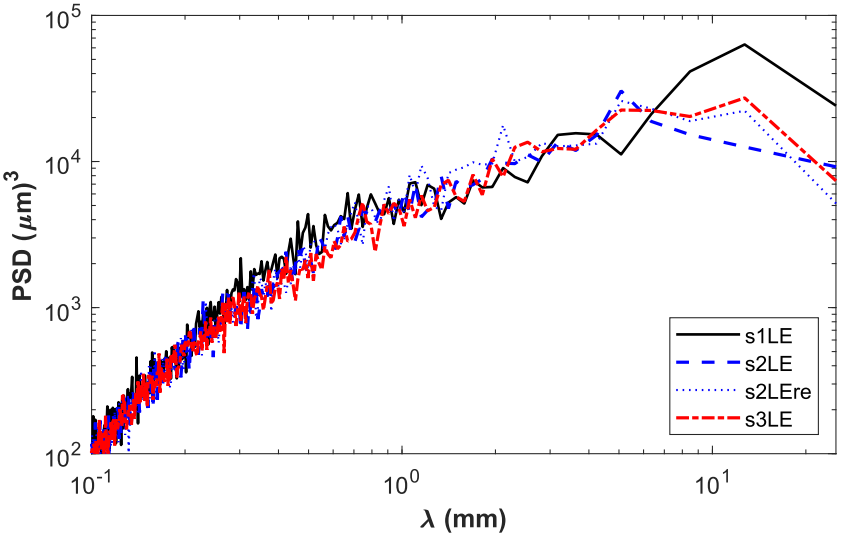

Figure 19: PSD comparison for full scans performed on the starboard wing near the leading edge and in the spanwise direction. Note that "s2LEre" represents repeated spanwise scans taken in the s2LE region.

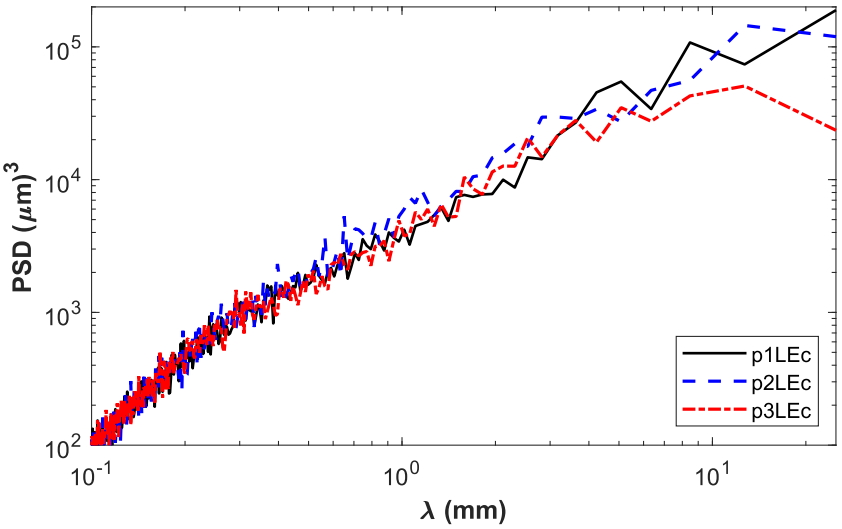

Figure 20: PSD comparison for full scans performed on the port wing near the leading edge and in the chordwise direction.

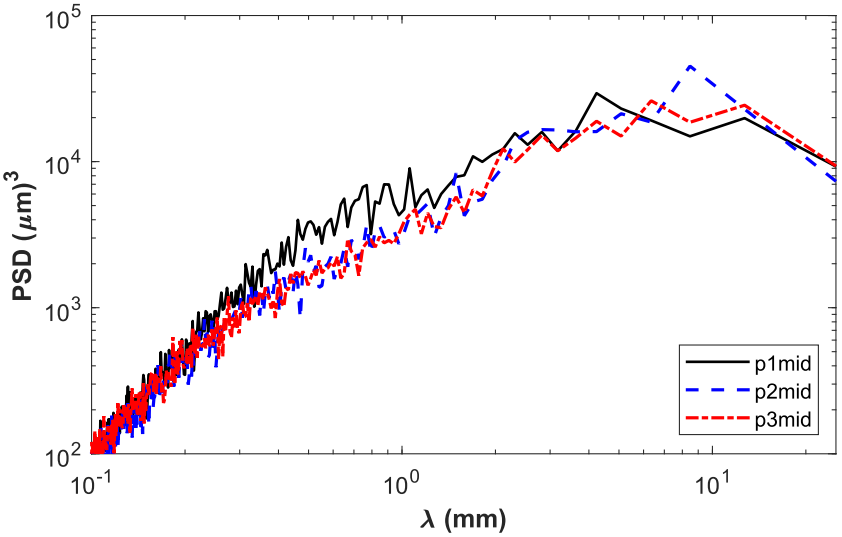

Figure 21: PSD comparison for full scans performed on the port wing near midchord and in the spanwise direction.

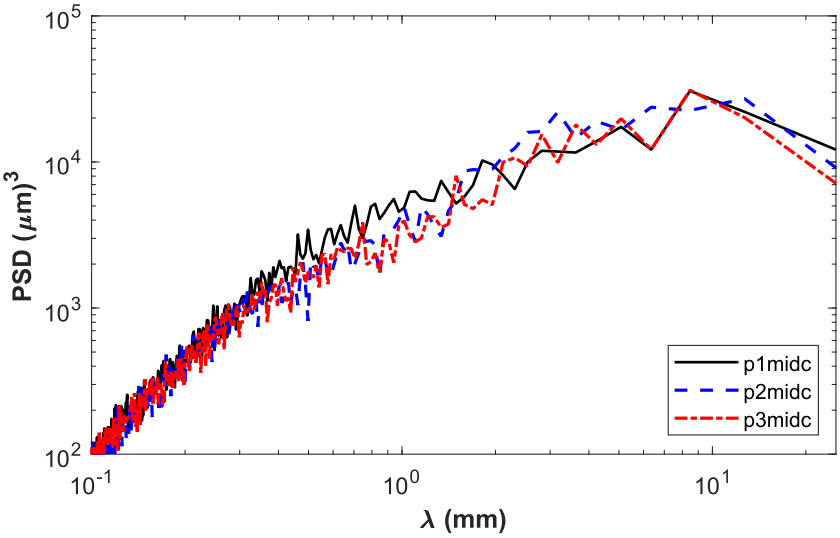

Figure 22: PSD comparison for full scans performed on the port wing near midchord and in the chordwise direction.

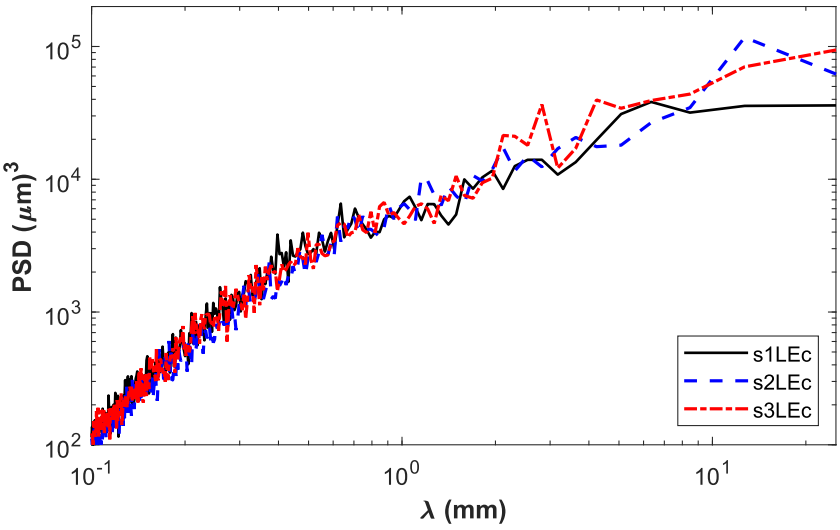

Figure 23: PSD comparison for full scans performed on the starboard wing near the leading edge and in the chordwise direction.

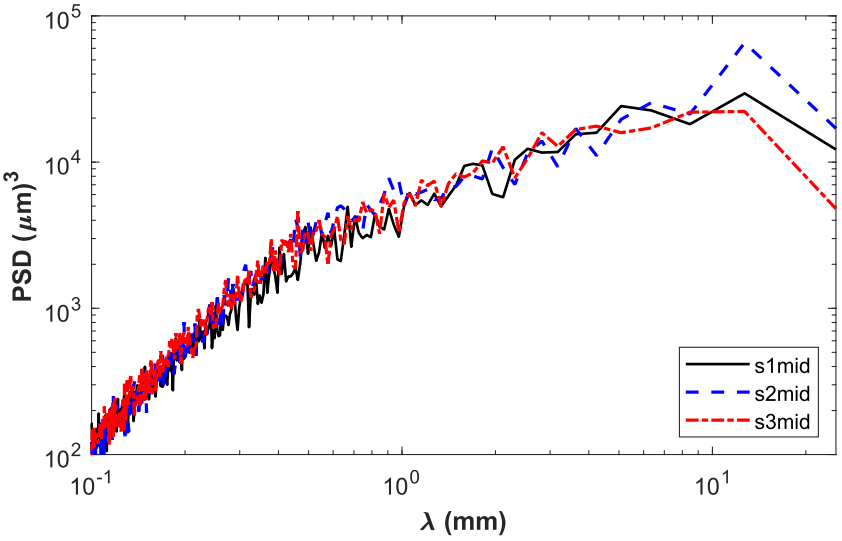

Figure 24: PSD comparison for full scans performed on the starboard wing near midchord and in the spanwise direction.

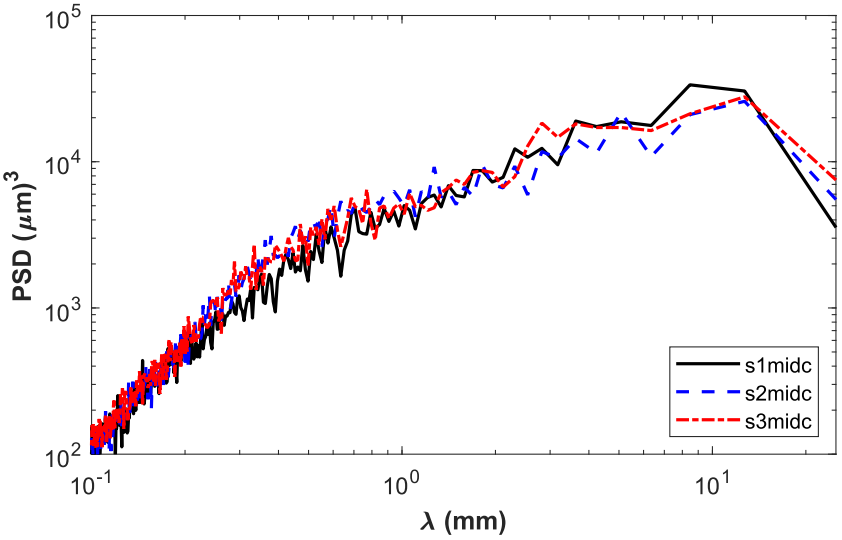

Figure 25: PSD comparison for full scans performed on the starboard wing near midchord and in the chordwise direction.

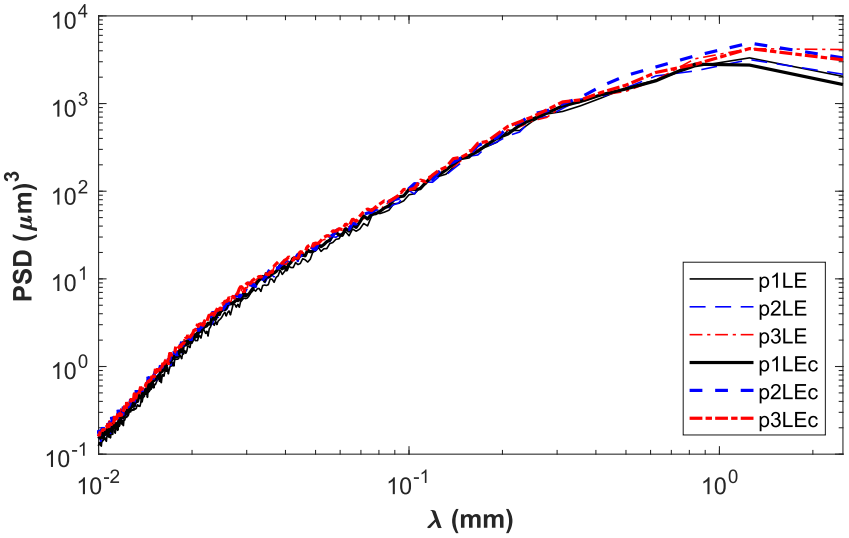

Figure 26: PSD comparison for sampling length scans performed on the port wing near the leading edge.

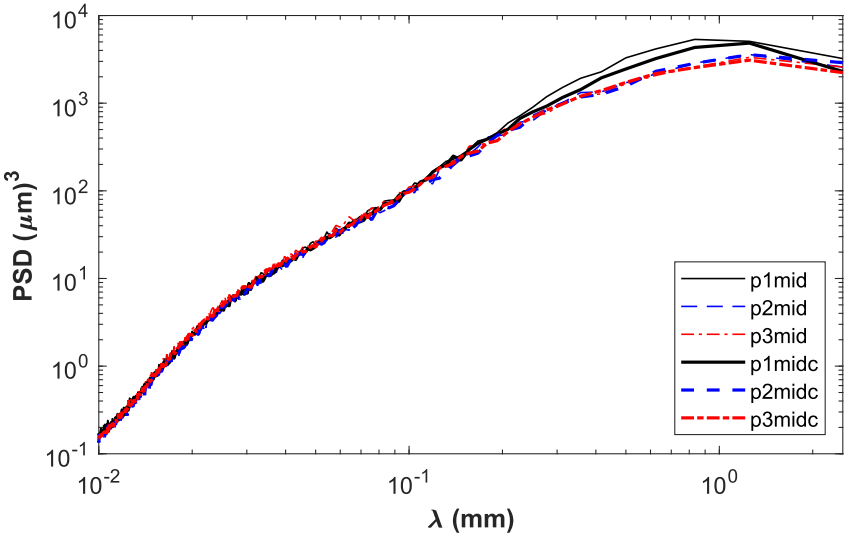

Figure 27: PSD comparison for sampling length scans performed on the port wing near the midchord.

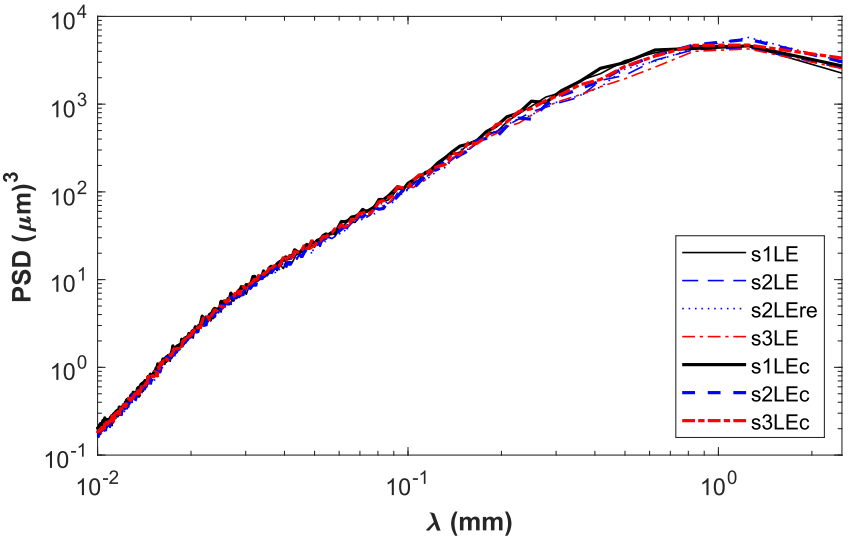

Figure 28: PSD comparison for sampling length scans performed on the starboard wing near the leading edge.

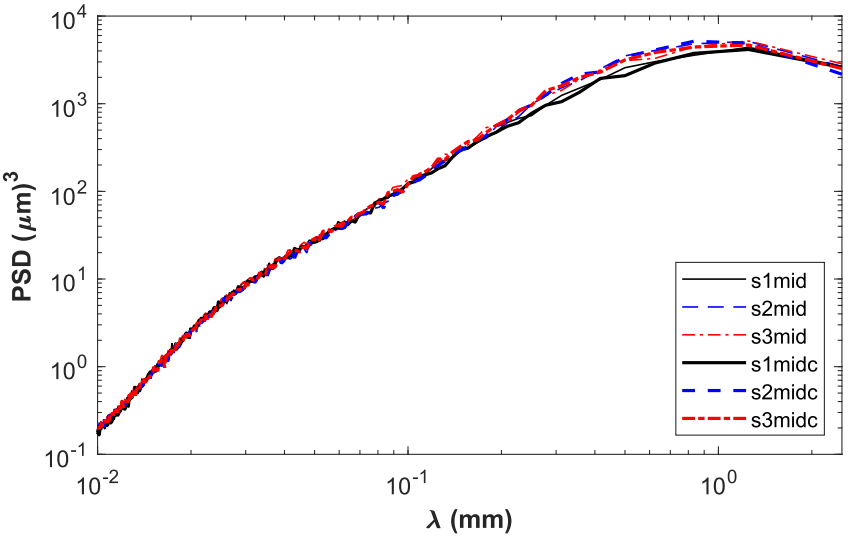

Figure 29: PSD comparison for sampling length scans performed on the starboard wing near the midchord.

REPORT DOCUMENTATION PAGE

Form Approved
OMB No. 0704–0188

The public reporting burden for this collection of information is estimated to average 1 hour per response, including the time for reviewing instructions, searching existing data sources, gathering and maintaining the data needed, and completing and reviewing the collection of information. Send comments regarding this burden estimate or any other aspect of this collection of information, including suggestions for reducing this burden, to Department of Defense, Washington Headquarters Services, Directorate for Information Operations and Reports (0704-0188), 1215 Jefferson Davis Highway, Suite 1204, Arlington, VA 22202-4302. Respondents should be aware that notwithstanding any other provision of law, no person shall be subject to any penalty for failing to comply with a collection of information if it does not display a currently valid OMB control number.
PLEASE DO NOT RETURN YOUR FORM TO THE ABOVE ADDRESS.

1. REPORT DATE *(DD-MM-YYYY)*	2. REPORT TYPE	3. DATES COVERED *(From - To)*
01-03-2025	Technical Memorandum	

4. TITLE AND SUBTITLE
Surface Roughness Measurements on the NASA Juncture Flow Model: 2022 Test Entry

5a. CONTRACT NUMBER

5b. GRANT NUMBER

5c. PROGRAM ELEMENT NUMBER

6. AUTHOR(S)
Leidy, A. N.

5d. PROJECT NUMBER

5e. TASK NUMBER

5f. WORK UNIT NUMBER

7. PERFORMING ORGANIZATION NAME(S) AND ADDRESS(ES)
NASA Langley Research Center
Hampton, Virginia 23681-2199

8. PERFORMING ORGANIZATION REPORT NUMBER
L–12456

9. SPONSORING/MONITORING AGENCY NAME(S) AND ADDRESS(ES)
National Aeronautics and Space Administration
Washington, DC 20546-0001

10. SPONSOR/MONITOR'S ACRONYM(S)
NASA

11. SPONSOR/MONITOR'S REPORT NUMBER(S)
NASA/TM–20250002895

12. DISTRIBUTION/AVAILABILITY STATEMENT
Unclassified-Unlimited
Subject Category 64
Availability: NASA STI Program (757) 864-9658

13. SUPPLEMENTARY NOTES
An electronic version can be found at http://ntrs.nasa.gov.

14. ABSTRACT

Surface roughness measurements were made on the upper surface of both wings of the NASA Juncture Flow model prior to its entry into the NASA Langley 14- by 22-Foot Subsonic Tunnel in January 2022. Measurements were acquired using a stylus profilometer with a 2-µm radius tip. Roughness parameters were evaluated in accordance with the ASME B46.1-2002 standards. The root-mean-square roughness levels, considering all measured regions, were 3.104 ± 0.016 µm and 3.532 ± 0.015 µm on the port and starboard wings, respectively. Roughness spectra were also provided since wavelengths between 3–5 mm were computationally shown to amplify the crossflow instability. More prominent spectral peaks were observed on the leading edge of the port wing compared to the starboard wing. Additional profiles were taken with the model installed in the tunnel following the boundary-layer transition measurements. The measurements within the tunnel focused on evaluating the step height and gap width at the interface between the wing and fairing.

15. SUBJECT TERMS
profilometry, surface roughness, step height, gap width, juncture flow, boundary layer transition, turbulence

16. SECURITY CLASSIFICATION OF:			17. LIMITATION OF ABSTRACT	18. NUMBER OF PAGES	19a. NAME OF RESPONSIBLE PERSON
a. REPORT	b. ABSTRACT	c. THIS PAGE			STI Information Desk (help@sti.nasa.gov)
U	U	U	UU	40	19b. TELEPHONE NUMBER *(Include area code)* (757) 864-9658